INTERNATIONAL JOURNAL FOR NUMERICAL METHODS IN ENGINEERING
Int. J. Numer. Meth. Engng 2007; **72**:253–294
Published online 19 February 2007 in Wiley InterScience (www.interscience.wiley.com). DOI: 10.1002/nme.1992

Diamond elements: A finite element/discrete-mechanics approximation scheme with guaranteed optimal convergence in incompressible elasticity

P. Hauret[1], E. Kuhl[2] and M. Ortiz[1,*,†]

[1]*Graduate Aeronautical Laboratories, California Institute of Technology, Pasadena, CA 91125, U.S.A.*
[2]*Technische Universität Kaiserslautern, Postfach 3049, Kaiserslautern D-67653, Germany*

SUMMARY

We present a finite element discretization scheme for the compressible and incompressible elasticity problems that possess the following properties: (i) the discretization scheme is defined on a triangulation of the domain; (ii) the discretization scheme is defined—and is identical—in all spatial dimensions; (iii) the displacement field converges optimally with mesh refinement; and (iv) the inf–sup condition is automatically satisfied. The discretization scheme is motivated both by considerations of topology and analysis, and it consists of the combination of a certain mesh pattern and a choice of interpolation that guarantees optimal convergence of displacements and pressures. Rigorous proofs of the satisfaction of the inf–sup condition are presented for the problem of linearized incompressible elasticity. We additionally show that the discretization schemes can be given a compelling interpretation in terms of discrete differential operators. In particular, we develop a discrete analogue of the classical tensor differential complex in terms of which the discrete and continuous boundary-value problems are formally identical. We also present numerical tests that demonstrate the dimension-independent scope of the scheme and its good performance in problems of finite elasticity. Copyright © 2007 John Wiley & Sons, Ltd.

Received 15 February 2006; Revised 11 August 2006; Accepted 23 October 2006

KEY WORDS: incompressible elasticity; inf–sup condition; macroelements; discrete mechanics

1. INTRODUCTION

In this paper, we present a finite element discretization scheme for the compressible and incompressible elasticity problems that possess the following properties: (i) the discretization scheme is defined on a triangulation of the domain (triangular meshes in two dimensions and tetrahedral meshes in three dimensions); (ii) the discretization scheme is defined—and is identical—in all

*Correspondence to: M. Ortiz, Graduate Aeronautical Laboratories, California Institute of Technology, Pasadena, CA 91125, U.S.A.
†E-mail: ortiz@aero.caltech.edu

spatial dimensions; (iii) the displacement field converges optimally with mesh refinement; and (iv) the inf–sup condition [1–3] is automatically satisfied and, consequently, the pressure field is free of checkerboard modes. The design of the discretization scheme acknowledges from the outset that two main factors determine performance, including convergence, in the incompressible or near-incompressible limit: (i) the topology of the mesh and (ii) the choice of displacement and pressure interpolation. Consideration of both factors in the design of a discretization scheme is essential and, in isolation, neither suffices to guarantee the optimal performance of the scheme.

This observation notwithstanding, the literature on finite elements for incompressible elasticity has emphasized either the choice of interpolation space or the choice of mesh topology but rarely both simultaneously.

The first line of inquiry has led to seminal contributions including: the concept of local bubble enrichment for the displacements first introduced by Crouzeix and Raviart [4] and analysed by Bercovier and Pironneau [5] and Verfürth [6], Arnold *et al*. [7] and others; Hughes's assumed-strain method [8], consisting of using different interpolations for the volumetric and deviatoric components of deformation; Simo and Rifai's [9] reformulation of Hughes' assumed-strain method based on the Hu–Washizu variational principle (cf. [10, 11] for recent related work); and others. Assumed strains have their niche between constant strain simplicial elements, to which they fail to apply, and second- or higher-order displacement interpolation, such as the Taylor–Hood $\mathbb{Q}_k/\mathbb{Q}_{k-1}$ elements or the $\mathbb{P}_k/\mathbb{P}_{k-1}$ elements, $k \geqslant 2$, which, as shown by Stenberg [12], require no enrichment (see also [5] and [13, p. 176] for the case $k=2$). Methods based on bubble enrichment for the displacements, such as the $\mathbb{P}_1$-bubble/$\mathbb{P}_1$ approach (cf., e.g. [14, 15]), are also popular due to their simplicity and good performance.

The second line of inquiry strives to identify special meshes whose particular topology results in convergent displacements or in the satisfaction of the inf–sup condition. Notable among these is the crossed-triangle approach of Nagtegaal *et al*. [16], further discussed and analysed by Mercier [17] and Kikuchi [18]. Crossed-triangle meshes are constructed by quadrisecting square meshes, and have convergence properties similar to the $\mathbb{Q}_1/\mathbb{Q}_0$ element. Another seminal contribution was made by Le Tallec [19], who discovered a special arrangement of quadrilaterals in two dimensions with the property that $\mathbb{Q}_1/\mathbb{Q}_0$ elements placed in that arrangement satisfy the inf–sup condition. This work was among the first to establish a clear connection between the inf–sup condition and the topology of the mesh. In subsequent years, that connection was sharpened and made precise by the macroelement analysis of Boland–Nicolaides [20, 21] and Stenberg [12, 22, 23].

The discretization scheme developed here is motivated both by considerations of topology and analysis. The key objective is to identify a combination of a mesh or 'tiling' pattern and a choice of interpolation that guarantee optimal convergence of displacements and pressures. In particular, that scheme should satisfy the inf–sup condition in the incompressible limit, and it should be flexible enough to allow general unstructured discretizations of the domain. A scheme that meets these requirements can be constructed as follows. We start from an arbitrary triangulation of the domain, or *primal mesh*, and append to its node set a collection of *dual nodes* located at the barycentres of the *primal elements*. We then proceed to subdivide every primal element into $d+1$ *sub-elements*, where d is the dimension of space, obtained by connecting the primal and the dual nodes. Finally, we pair the sub-elements resulting from subdivision along all the *primal faces* to define *diamond elements*. These elements thus consist of pairs of sub-elements sharing a primal face and contain d primal nodes and two dual nodes, or a total of $d+2$ nodes. This completes the topological reworking of the primal mesh. We then proceed to define interpolation spaces for displacements and pressure based on the diamond mesh. For definiteness, we choose piecewise-linear

DOI: 10.1002/nme

displacement interpolation on sub-elements and constant pressure interpolation on diamond elements. The interpolation spaces are chosen with a view to satisfying the inf–sup condition.

We additionally explore the alternative point of view of *discrete mechanics*, and show that the diamond approximation scheme can be given a compelling and illuminating interpretation as a discrete mechanics scheme. Discrete mechanics may be regarded as a self-contained theory of deformable solids in which space—and possibly time—is discrete *ab initio*. The central goal is to define a *discrete differential complex* on a discretization of the domain such that the discrete boundary-value problem, when expressed in terms of discrete differential operators, is identical to the continuum, or *classical*, boundary-value problem.

However, whereas the differential complex that underlies potential theory, electromagnetism and other vector field theories in $\mathbb{R}^3$, namely the classical de Rham complex with its familiar differential operators grad, curl and div, is well-known, the differential complex underlying *tensor* field theories such as linear elasticity seems to have remained cloaked in relative obscurity. The three-dimensional tensor differential complex was fully developed in connection with linear-elastic dislocation theory by Kröner [24] and its differential operators are: the deformation operator Def; the incompatibility operator Inc; and the tensor-divergence operator Div. In keeping with the relative obscurity of this tensor complex, whereas the formulation of *discrete* differential complexes has received considerable attention in the context of vector field theories (cf., e.g. [25–29], and reference therein), the formulation of discrete *tensor* differential complexes as a discretization tool has received much less attention. A notable exception is the recent work of Arnold *et al.* [30–33], which has led to the formulation of discrete differential complexes and mixed stress–displacement interpolation schemes well-suited to applications in compressible elasticity.

We formulate a complete *discrete tensor differential complex*, whose properties mirror closely those of the classical tensor differential complex, such that the corresponding discrete boundary value problem is identical to that which is obtained by means of the diamond approximation scheme. This correspondence shows that the diamond approximation scheme, which is defined in terms of interpolation and Galerkin reduction, is, in effect, a discrete mechanics scheme. We show that the discrete tensor differential operators Def, Inc and Div have adjointness properties. We prove that they give rise to a Helmholtz–Hodge decomposition of symmetric tensor fields and define a tensor cohomology and tensor-harmonic functions. A key step in connecting the diamond approximation scheme and discrete mechanics is the definition of a suitable metric. This metric entails a certain averaging of volumetric deformations that is ultimately responsible for the satisfaction of the inf–sup condition. The introduction of a metric in turn permits the definition of a discrete *isotropic* differential complex that is key to the formulation of the discrete boundary-value problem of incompressible linear elasticity. The discrete isotropic differential complex carries a cohomology of its own, and we show that the inf–sup condition is equivalent to the requirement that a certain cohomology group be trivial. This establishes a far-reaching connection between discrete topology and analysis, and confirms the intuition among practitioners that the topology—or *layout*—of a mesh, as well as the choice of interpolation, has a direct and equally important bearing on the convergence characteristics of an approximation scheme. From this point of view, the diamond scheme may be regarded as a particular choice of mesh—or *tiling*—pattern which ensures that the topology of the mesh is 'right'.

Despite the appeal of discrete mechanics, it bears emphasis that considerations of discrete geometry alone do not guarantee that a discretization scheme is convergent. In particular, counterexamples [34] show that there are approximation schemes that are expressible in terms of well-defined discrete differential complexes but which fail to converge in general. These counter

DOI: 10.1002/nme

examples demonstrate that considerations of analysis, such as the inf–sup condition, as well as considerations of discrete geometry should play a role in the design of approximation schemes.

The paper is organized as follows. We prove in Section 2 that the inf–sup condition is automatically satisfied by the diamond scheme, which in turn ensures checkerboard-free convergence of the pressure field. In Section 3, we develop the discrete tensor differential complex, including a suitable metric, establish its main properties and show how it relates to the diamond scheme and to the inf–sup condition. The results of the analysis are born out by the numerical tests presented in Section 4.1. These tests additionally demonstrate the dimension-independent scope of the scheme, which can be formulated with equal ease in two, three or any arbitrary spatial dimensions, and its good performance in problems of finite elasticity.

2. PROBLEM SETTING AND ANALYSIS

Of key concern as regards analysis is the behaviour of approximation schemes in the presence of internal constraints such as incompressibility. The analysis tools required for elucidating such behaviour are best developed for linear problems. In consequence, we begin by describing diamond elements and analysing their behaviour in the linear regime. Specifically, we choose linear elasticity as a convenient model problem in that regime. Extensions of the approach to non-linear problems are presented in Section 4.1.

2.1. Linearized elasticity

We begin by collecting relevant results from analysis for subsequent reference and with a view to establishing our notation. We consider an elastic solid occupying a domain $\Omega \subset \mathbb{R}^d$, which is assumed to be *polygonal* for the sake of simplicity. The solid deforms under the action of tractions $t \in L^2(\Gamma_N)^d$ distributed over the Neumann boundary $\Gamma_N \subset \partial\Omega$, and of body forces $f \in L^2(\Omega)^d$. For simplicity, we assume that the displacements vanish on the Dirichlet boundary $\Gamma_D = \partial\Omega \backslash \Gamma_N$. We additionally confine attention to uniform linear isotropic materials characterized by finite Lamé constants $\lambda > 0$ and $\mu > 0$. The bulk modulus of the material is $\kappa = \lambda + 2\mu/3$.

We shall be particularly interested in the behaviour of solutions u^ε under the scaling λ/ε, $\varepsilon \to 0$, corresponding to the incompressible limit. In variational form, the problem is to find the displacement field $u^\varepsilon \in H^1_*(\Omega)$ such that

$$a(u^\varepsilon, v) + \varepsilon^{-1} \int_\Omega \operatorname{div} u^\varepsilon \operatorname{div} v = l(v) \quad \forall v \in H^1_*(\Omega) \tag{1}$$

In this statement, $H^1_*(\Omega) := \{v \in H^1(\Omega)^d, v = 0 \text{ on } \Gamma_D\}$ is the space of admissible displacement fields and we have introduced the bilinear and linear forms

$$a(u, v) = \int_\Omega 2\mu\varepsilon(u) : \varepsilon(v) \tag{2a}$$

$$l(v) = \int_\Omega f \cdot v + \int_{\Gamma_N} t \cdot v \tag{2b}$$

DOI: 10.1002/nme

which are independent of ε. Here and subsequently, $\xi : \zeta = \xi_{ij}\zeta_{ij}$ denotes the inner product between two matrices, and $u \cdot v$ denotes the inner product of vectors. In addition, $\varepsilon(u) = (\nabla u + (\nabla u)^{\mathrm{t}})/2$ is the strain operator and, for simplicity of notation, we have chosen units such that $\lambda = 1$.

We recall (cf., e.g. [35]) that Korn's inequality ensures the coercivity of a, i.e. there exists a constant $\alpha > 0$ such that

$$a(v, v) \geqslant \alpha \|v\|_{1,\Omega}^2 \quad \forall v \in H_*^1(\Omega) \tag{3}$$

and the existence and uniqueness of solutions of problem (1) follows from the Lax–Milgram lemma. In addition, the solution depends continuously on the data, i.e.

$$\|u^\varepsilon\|_{1,\Omega} \leqslant C(\|f\|_{0,\Omega} + \|t\|_{0,\Gamma_{\mathrm{N}}}) \tag{4}$$

where the constant $C > 0$ is independent of the loading and the Lamé constants. In the above statements we have introduced the standard L^2 and H^1 norms

$$\|v\|_{0,\Omega} = \left(\int_\Omega |v|^2 \right)^{1/2} \tag{5a}$$

$$\|v\|_{1,\Omega} = (\|v\|_{0,\Omega}^2 + \|\nabla v\|_{0,\Omega}^2)^{1/2} \tag{5b}$$

Denoting by p^ε the pressure

$$p^\varepsilon = \varepsilon^{-1} \operatorname{div} u^\varepsilon \tag{6}$$

(1) can be restated as the problem of finding $u^\varepsilon \in H_*^1(\Omega)$ and $p^\varepsilon \in L^2(\Omega)$ such that

$$\begin{aligned} a(u^\varepsilon, v) + b(v, p^\varepsilon) &= l(v) \qquad \forall v \in H_*^1(\Omega) \\ b(u^\varepsilon, q) &= \varepsilon(p^\varepsilon, q)_\Omega \quad \forall q \in L^2(\Omega) \end{aligned} \tag{7}$$

where we have introduced the additional bilinear forms

$$b(v, q) = \int_\Omega q \operatorname{div} v \tag{8a}$$

$$(p, q)_\Omega = \int_\Omega pq \tag{8b}$$

We recall that, for Dirichlet boundary conditions, $\Gamma_{\mathrm{D}} = \partial\Omega$, a standard application of the De Rham theorem [13, 14] results in the inf–sup inequality

$$\inf_{q \in L_0^2(\Omega)\setminus\{0\}} \sup_{v \in H_0^1(\Omega)^d \setminus \{0\}} \frac{\int_\Omega q \operatorname{div} v}{\|v\|_{1,\Omega} \|q\|_{0,\Omega}} \geqslant \beta > 0 \tag{9}$$

where we write $H_0^1(\Omega) := \{v \in H^1(\Omega),\ v = 0 \text{ on } \partial\Omega\}$ and $L_0^2(\Omega) := \{q \in L^2(\Omega),\ \int_\Omega q = 0\}$. More generally, in the case of mixed boundary conditions, $\Gamma_{\mathrm{D}} \neq \partial\Omega$, using a lifting argument (cf., e.g.

DOI: 10.1002/nme

[14, Lemma 4.9, p. 181]) and assuming that Γ_D is polyhedral, the following inf–sup inequality holds:

$$\inf_{q\in L^2(\Omega)\setminus\{0\}} \sup_{v\in H^1_*(\Omega)\setminus\{0\}} \frac{\int_\Omega q \operatorname{div} v}{\|v\|_{1,\Omega}\|q\|_{0,\Omega}} \geqslant \beta > 0 \tag{10}$$

The following theorem establishes the existence and uniqueness of solutions and their behaviour in the incompressible limit (cf., e.g. [14, Theorem 4.3, p. 178; Proposition 4.44, p. 211]).

Theorem 1
For every $0\leqslant\varepsilon\leqslant\infty$, problem (7) admits a unique solution $(u^\varepsilon, p^\varepsilon)\in H^1_*(\Omega)\times L^2(\Omega)$ such that

$$\|u^\varepsilon\|_{1,\Omega} + \|p^\varepsilon\|_{0,\Omega} \leqslant C(\|f\|_{0,\Omega} + \|t\|_{0,\Gamma_N}) \tag{11}$$

uniformly in ε. Moreover,

$$\|u^\varepsilon - u^0\|_{1,\Omega} + \|p^\varepsilon - p^0\|_{0,\Omega} \leqslant C\varepsilon(\|f\|_{0,\Omega} + \|t\|_{0,\Gamma_N}) \tag{12}$$

In particular, $(u^\varepsilon, p^\varepsilon)\to(u^0, p^0)$ in $H^1_*(\Omega)\times L^2(\Omega)$ as $\varepsilon\to 0$.

2.2. General issues of discretization

In this section, we briefly review relevant results of analysis pertaining to the discretization of problem (7); (cf., e.g. [13–15] for a complete account). We begin by specifying two sequences of finite-dimensional spaces, $\mathsf{V}_h\subset H^1_*(\Omega)$ and $\mathsf{P}_h\subset L^2(\Omega)$, equipped with the subspace topology. The discretization of (7) is then effected by restricting displacements to $\mathsf{V}_h\subset H^1_*(\Omega)$ and pressures to $\mathsf{P}_h\subset L^2(\Omega)$, along with their variations. In the displacement finite element method, consisting of the constrained minimization of the potential energy over V_h, the space of discrete pressure fields is, by default,

$$\mathsf{P}_h = \{\operatorname{div} v_h,\ v_h\in\mathsf{V}_h\} \tag{13}$$

With $0<\varepsilon<+\infty$, the discrete linearized elasticity problem consists of finding $u^\varepsilon_h\in\mathsf{V}_h$ and $p^\varepsilon_h\in\mathsf{P}_h$ such that

$$\begin{aligned} a(u^\varepsilon_h, v_h) + b(v_h, p^\varepsilon_h) &= l(v_h) \qquad \forall v_h\in\mathsf{V}_h \\ b(u^\varepsilon_h, q_h) &= \varepsilon(p^\varepsilon_h, q_h) \quad \forall q_h\in\mathsf{P}_h \end{aligned} \tag{14}$$

Since V_h is a subspace of $H^1_*(\Omega)$, problem (14) retains coercivity, which in turn ensures existence and uniqueness of discrete solutions. The stability estimate

$$\|u^\varepsilon_h\|_{1,\Omega} \leqslant C(\|f\|_{0,\Omega} + \|t\|_{0,\Gamma_N}) \tag{15}$$

additionally holds, with constant $C>0$ independent of ε. It follows from this estimate that, for fixed h, the sequence u^ε_h is uniformly bounded in ε and, hence, there exists a subsequence that converges in V_h. A standard exercise shows that the limit of that subsequence is indeed a solution of the incompressible discrete problem

$$\begin{aligned} a(u^0_h, v_h) + b(v_h, p^0_h) &= l(v_h) \quad \forall v_h\in\mathsf{V}_h \\ b(u^0_h, q_h) &= 0 \qquad \forall q_h\in\mathsf{P}_h \end{aligned} \tag{16}$$

DOI: 10.1002/nme

Unfortunately, for an arbitrary choice of P_h, the only solution to this problem may be $u_h^0 = 0$, a phenomenon known as *volumetric locking*. In particular, the default choice (13) is often afflicted by this pathology.

Problem (16) can be reformulated as

$$a(u_h^0, v_h) = l(v_h) \quad \forall v_h \in \mathfrak{V}_h \tag{17}$$

where

$$\mathfrak{V}_h = \{v_h \in \mathsf{V}_h, b(v_h, q_h) = 0, \forall q_h \in \mathsf{P}_h\} \tag{18}$$

Evidently, $\mathfrak{V}_h = \operatorname{Ker} \mathscr{B}_h$ with $\mathscr{B}_h : v_h \in \mathsf{V}_h \to \mathsf{P}_h' \ni b(v_h, \cdot)$, where P_h' is the dual of P_h. In view of (16), we have that $a(u_h^0, \cdot) - l(\cdot) \in (\operatorname{Ker} \mathscr{B}_h)^\perp = \operatorname{Im}(\mathscr{B}_h^{\mathrm{t}})$. Therefore, there exists a discrete pressure field $p_h^0 \in \mathsf{P}_h$ such that

$$a(u_h^0, v_h) + b(v_h, p_h^0) = l(v_h) \quad \forall v_h \in \mathsf{V}_h \tag{19}$$

However, p_h^0 is uniquely determined only if

$$b(v_h, q_h) = 0 \quad \forall v_h \in \mathsf{V}_h \;\Rightarrow\; q_h = 0 \tag{20}$$

i.e. if $\operatorname{Ker}(\mathscr{B}_h^{\mathrm{t}}) = \{0\}$, which in turn implies that $\operatorname{Im} \mathscr{B}_h = \mathsf{V}_h$. It is equivalent to the discrete inf–sup condition:

$$\inf_{q_h \in \mathsf{P}_h \setminus \{0\}} \sup_{v_h \in \mathsf{V}_h \setminus \{0\}} \frac{b(v_h, q_h)}{\|q_h\|_{0,\Omega} \|v_h\|_{1,\Omega}} \geqslant \beta_h > 0 \tag{21}$$

If this condition is not satisfied with β_h uniformly bounded below by a positive constant independent of h, then the sequence p_h^ε is not uniformly bounded as $\varepsilon \to 0$ in general. In practice, the component of p_h^ε in $\operatorname{Ker}(\mathscr{B}_h^{\mathrm{t}}) \setminus \{0\}$ may blow up as $\varepsilon \to 0$, and this divergence manifests itself in the form of spurious 'checkerboard' modes that corrupt the solution. By way of sharp contrast, the behaviour of the solution when the discrete inf–sup condition uniformly holds is characterized by the following theorem (cf., e.g. [14]).

Theorem 2

Suppose that there exits a constant $\beta > 0$ independent of h such that the inf–sup (21) is satisfied with $\beta_h \geqslant \beta$ for all $h > 0$. Then, for all $h > 0$ and $0 \leqslant \varepsilon \leqslant +\infty$, problem (14) admits a unique solution $(u_h^\varepsilon, p_h^\varepsilon) \in \mathsf{V}_h \times \mathsf{P}_h$ such that

$$\|u_h^\varepsilon\|_{1,\Omega} + \|p_h^\varepsilon\|_{0,\Omega} \leqslant C(\|f\|_{0,\Omega} + \|t\|_{0,\Gamma_{\mathrm{N}}}) \tag{22}$$

uniformly in h, ε. Moreover,

$$\|u_h^\varepsilon - u_h^0\|_{1,\Omega} + \|p_h^\varepsilon - p_h^0\|_{0,\Omega} \leqslant C\varepsilon(\|f\|_{0,\Omega} + \|t\|_{0,\Gamma_{\mathrm{N}}}) \tag{23}$$

In addition, if $(u^\varepsilon, p^\varepsilon) \in H^1_*(\Omega) \times L^2(\Omega)$ is solution of (7) with $0 \leqslant \varepsilon \leqslant +\infty$, then

$$\|u_h^\varepsilon - u^\varepsilon\|_{1,\Omega} + \|p_h^\varepsilon - p^\varepsilon\|_{0,\Omega} \leqslant C \left(\inf_{v_h \in \mathsf{V}_h} \|v_h - u^\varepsilon\|_{1,\Omega} + \inf_{q_h \in \mathsf{P}_h} \|q_h - p^\varepsilon\|_{0,\Omega} \right) \tag{24}$$

All the constants in the preceding estimates are independent of the loading, the elastic constants and h.

DOI: 10.1002/nme

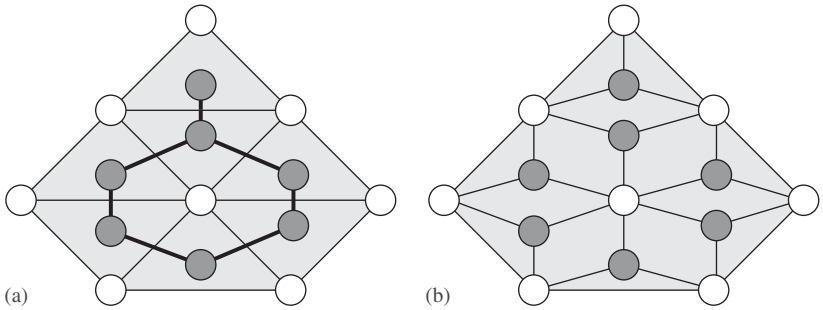

Figure 1. (a) Simplicial mesh $\mathscr{T}_h$ of a pentagonal domain (white circles) and dual node set $\mathscr{T}_h^*$ (grey circles) and (b) associated diamond mesh.

2.3. Diamond meshes

Next, we introduce a special class of conforming meshes that are derived from conventional triangulations of the domain and that form the basis for subsequent developments.

Suppose that we are given a triangulation of the *polygonal* domain $\Omega \subset \mathbb{R}^d$ $(d = 2, 3)$ of interest, to be termed the *primal* triangulation. Let $\mathscr{N}_h$ be the nodal or vertex set and $\mathscr{T}_h$ be the collection of d-simplices, or elements, in the primal triangulation. By a *face* of an element $T \in \mathscr{T}_h$ we shall specifically mean a $(d-1)$-face of T, i.e. a triangle for $d = 3$ and a segment for $d = 2$. We additionally denote by $\mathscr{F}_h$ the set of faces of $\mathscr{T}_h$, and by ∂T the collection of faces of element T.

The *diamond mesh* generated by $\mathscr{T}_h$ is constructed as follows. For every element $T \in \mathscr{T}_h$ we choose a point, T^*, to be termed the *dual node* of T, in its interior. For instance, T^* may conveniently be chosen as the barycentre of the simplex T. The dual nodal set is then the collection of all dual nodes, namely, $\mathscr{T}_h^* = \{T^*, T \in \mathscr{T}_h\}$. In addition, for every face $F \in \mathscr{F}_h$, we define its dual edge F^* to be the set of dual nodes adjacent to F. If F is an interior face, then F^* consists of two dual nodes and may be regarded as a segment. If F is a boundary face then F^* contains one single dual node and may be regarded as a ray. The dual edge set is then the collection of all dual edges, namely, $\mathscr{F}_h^* = \{F^*, F \in \mathscr{F}_h\}$. The *diamond element* $K(F)$ of a face $F \in \mathscr{F}_h$ is the convex hull of $\{F, F^*\}$, i.e. the polytope defined by F and its adjacent dual nodes. Thus, if F is an interior face, $K(F)$ is a bi-triangle for $d = 2$ and a bi-tetrahedron for $d = 3$. If F is a boundary face, $K(F)$ coincides with the unique d-simplex incident to F. We now define the *diamond mesh* generated by $\mathscr{T}_h$ as the mesh of nodal set $\mathsf{N}_h = \mathscr{N}_h \cup \mathscr{T}_h^*$ and element set $\mathsf{T}_h = \{K(F), F \in \mathscr{F}_h\}$. The geometry of a two-dimensional diamond mesh is illustrated in Figure 1.

It follows from the preceding construction that the nodal set of a diamond mesh consists of the union of the primal and dual nodes; and that its element set is the collection of the diamond elements corresponding to all the primal faces. However, it should be carefully noted that diamond meshes contain neither the primal nor the dual mesh. Instead, they *interpolate* between the primal and dual nodal sets.

2.4. Approximation spaces and analysis

Diamond meshes can be taken as a basis for constructing finite element approximations enjoying optimal convergence and stability properties. We take linearized elasticity as a convenient model problem (cf. Section 2.1), with particular focus on the behaviour of the solutions in the incompressible limit.

DOI: 10.1002/nme

We begin by introducing the displacement approximation space

$$\mathsf{V}_h = \{v \in H^1_*(\Omega),\, v|_K \in \mathsf{R}(K)^d,\, \forall K \in \mathsf{T}_h\} \tag{25}$$

where

$$\mathsf{R}(K(F)) = \{v \in H^1(K),\, v|_{[F,N]} \in \mathbb{P}_1([F,N]),\, N \in F^*\} \tag{26}$$

Here, $\mathbb{P}_1(T)$ is the space of polynomials of order $\leqslant 1$ over the simplex T; and $[F, N]$ denotes the simplex defined by a face F and a node N. Thus, $\mathsf{R}(K(F))$ consists of all linear polynomials on each of the constituent simplices $\{[F, N], N \in F^*\}$ of $K(F)$. With a view to analysing the incompressible limit, we additionally introduce the pressure space

$$\mathsf{P}_h = \{p \in L^2(\Omega),\, p|_K \in \mathbb{P}_0(K),\, \forall K \in \mathsf{T}_h\} \tag{27}$$

where $\mathbb{P}_0(T)$ is the space of constant functions over the simplex T. We also consider the subspaces

$$\mathsf{V}^0_h = \{v \in H^1_0(\Omega),\, v|_K \in \mathsf{R}(K)^d,\, \forall K \in \mathsf{T}_h\} \tag{28}$$

and

$$\mathsf{P}^0_h = \left\{p \in L^2(\Omega),\, \int_\Omega p = 0,\, p|_K \in \mathbb{P}_0(K),\, \forall K \in \mathsf{T}_h\right\} \tag{29}$$

We note in passing that when $\Gamma_{\mathrm{D}} = \partial\Omega$, the pressure field is determined up to an additive constant, and the solution (u, p) must be restricted to $H^1_0(\Omega) \times L^2_0(\Omega)$, or to $\mathsf{V}^0_h \times \mathsf{P}^0_h$ in the discrete case, in order to recover uniqueness of the pressure field.

Next, we exploit the special topology of diamond meshes in order to prove that the inf–sup condition is satisfied for the pair of spaces $\{\mathsf{V}^0_h, \mathsf{P}^0_h\}$. The method of proof relies on the macroelement technique of Boland–Nicolaides [20, 21] and Stenberg [12, 22, 23]. Thus, for every primal element $T \in \mathscr{T}_h$, we define the *macroelement*

$$M(T) := \bigcup_{F \in \partial T} K(F) = \bigcup_{F \in \partial T} \bigcup_{N \in F^*} [F, N] \tag{30}$$

Typical two- and three-dimensional macroelements are shown in Figures 2 and 3, respectively. In dimension d, there are $d+2$ types of macroelements, depending on whether $T \in \mathscr{T}_h$ has $0, 1, \ldots, d$ or $d+1$ faces on the boundary of Ω. By way of illustration, Figure 4 depicts the four possible types of macroelements in two dimensions. We also identify the unit regular d-simplex $\hat{T}$ as a reference simplex, and introduce the corresponding macroelements $\hat{M}$ defined by reflecting the dual node $\hat{T}^*$, which we take to coincide with the barycentre of $\hat{T}$, with respect to the faces of $\hat{T}$ (cf. Figure 4). We shall denote by $\mathfrak{M}$ the set of $d+2$ reference macroelements thus defined. The spaces

$$\hat{\mathsf{V}}^0_h(\hat{M}) = \{v_h \in H^1_0(\hat{M})^d,\, v_h|_{\hat{K}} \in \mathsf{R}(\hat{K})^d,\, \forall \hat{K} \in \hat{M}\} \tag{31}$$

and

$$\hat{\mathsf{P}}_h(\hat{M}) = \{q_h \in L^2(\hat{M}),\, q_h|_{\hat{K}} \in \mathbb{P}_0(\hat{K}),\, \forall \hat{K} \in \hat{M}\} \tag{32}$$

play a central role in subsequent developments.

DOI: 10.1002/nme

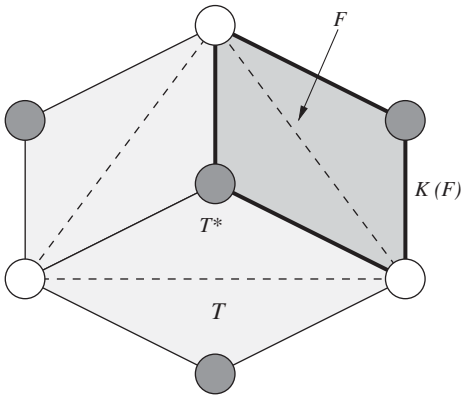

Figure 2. Detail of a two-dimensional macroelement (in thick lines) generated by the simplex $T \in \mathscr{T}_h$ (in dashed lines).

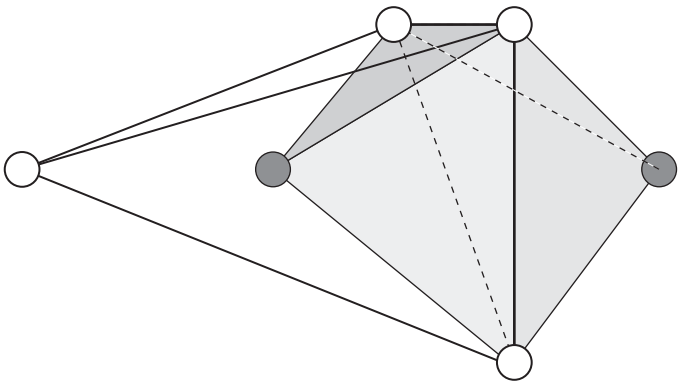

Figure 3. Partial representation of a three-dimensional macroelement based on a 4-node tetrahedron (white vertices and thick lines); only one of the four diamonds, based on the additional grey vertices, is represented.

Lemma 1
Let $\hat{M} \in \mathfrak{M}$ be a macroelement and $q_h \in \hat{\mathsf{P}}_h(\hat{M})$. Suppose that

$$\int_{\hat{M}} q_h \operatorname{div} v_h = 0 \quad \forall v_h \in \hat{\mathsf{V}}_h^0(\hat{M}) \tag{33}$$

Then $q_h = \text{constant}$.

Proof
We begin by noting that $\hat{\mathsf{V}}_h^0(\hat{M})$ consists of functions of the form: $v_h = \alpha\phi$ with $\alpha \in \mathbb{R}^d$ and ϕ the piecewise linear continuous function that takes the values 1 at the centre dual node $\hat{T}^*$ and

DOI: 10.1002/nme

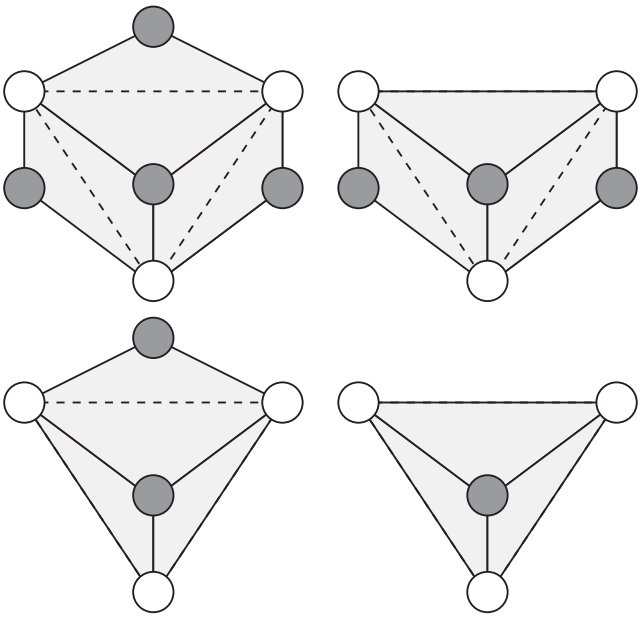

Figure 4. The four types of two-dimensional macroelements. The triangle that generates the macroelement is shown in dashed lines.

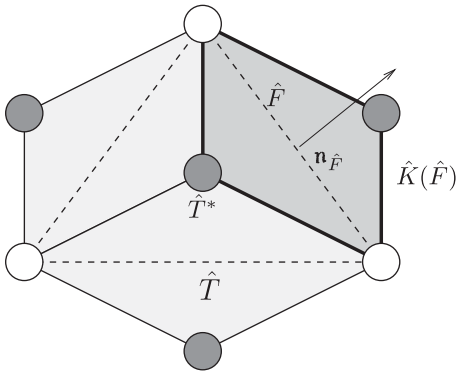

Figure 5. Detail of the notation used in the proof for a typical reference macroelement $\hat{M} \in \mathfrak{M}$ in two dimensions.

0 at all the remaining nodes of $\hat{M}$. Let $q_h \in \hat{\mathsf{P}}_h(\hat{M})$. Then,

$$\int_{\hat{M}} q_h \operatorname{div} v_h = \sum_{\hat{F}\in\partial\hat{T}} q_h|_{\hat{K}(\hat{F})} \int_{\hat{K}(\hat{F})} \alpha \cdot \nabla\phi = \sum_{\hat{F}\in\partial\hat{T}} q_h|_{\hat{K}(\hat{F})} \int_{\hat{K}(\hat{F})\cap\hat{T}} \alpha \cdot \nabla\phi$$

$$= \frac{1}{d} \sum_{\hat{F}\in\partial\hat{T}} q_h|_{\hat{K}(\hat{F})} |\hat{F}| \alpha \cdot n_{\hat{F}} \tag{34}$$

DOI: 10.1002/nme

where, here and subsequently, $|\cdot|$ denotes the measure of a set, and $n_{\hat{F}}$ is the outward unit normal to $\hat{F}$. Suppose that (33) holds. Then, by (34),

$$\sum_{\hat{F}\in\partial\hat{T}} q_h|_{\hat{K}(\hat{F})}|\hat{F}|n_{\hat{F}}=0 \tag{35}$$

Consider the linear mapping $A\in\mathscr{L}(\hat{\mathsf{P}}_h(\hat{M});\mathbb{R}^d)$ defined by

$$A(q_h)=\sum_{\hat{F}\in\partial\hat{T}} q_h|_{\hat{K}(\hat{F})}|\hat{F}|n_{\hat{F}} \quad \forall q_h\in\hat{\mathsf{P}}_h(\hat{M}) \tag{36}$$

Then, condition (35) is equivalent to requiring that $q_h\in\ker(A)$, where $\ker(A)$ is the kernel of A. But $\ker(A)=\mathrm{im}(A^{\mathrm{t}})^{\perp}$, where $\mathrm{im}(A^{\mathrm{t}})$ is the range of adjoint mapping A^{t} and $\mathrm{im}(A^{\mathrm{t}})^{\perp}$ its orthogonal complement. Since any d of the vectors $|\hat{F}|n_{\hat{F}}$ are linearly independent, it follows that $\dim\mathrm{im}(A^{\mathrm{t}})=d$ and, hence, $\dim\ker(A)=1$. Since

$$\sum_{\hat{F}\in\partial\hat{T}} |\hat{F}|n_{\hat{F}}=0$$

it follows that functions $q_h=$constant belong to $\ker(A)$ and, thus, $\ker(A)$ equals the constant members of $\hat{\mathsf{P}}_h(\hat{M})$. □

Proposition 1
For $d=2$, 3, there exists a constant $\beta_0>0$ independent of the mesh size $h>0$ such that

$$\inf_{q_h\in\mathsf{P}_h^0\setminus\{0\}}\sup_{v_h\in\mathsf{V}_h^0\setminus\{0\}}\frac{\int_\Omega q_h\,\mathrm{div}\,v_h}{\|q_h\|_{0,\Omega}\|v_h\|_{1,\Omega}}\geqslant\beta_0 \tag{37}$$

Proof
With reference to Figure 1, we note the following properties of macroelements:

(i) Every diamond element $D\in\mathsf{T}_h$ belongs to at least one macroelement, and at most two.
(ii) A face of a diamond is contained in the interior of one and only one macroelement.
(iii) For every primal element $T\in\mathscr{T}_h$, there exists a reference macroelement $\hat{M}\in\mathfrak{M}$ and a continuous one-to-one mapping $g:\hat{M}\to M(T)$ with the following properties:

(iiia) g is a simplicial map, i.e. it maps the simplices of $\hat{M}$ to the simplices of $M(T)$;
(iiib) g is piecewise linear, i.e. $g|_{[\hat{F},\hat{N}]}\in\mathbb{P}_1([\hat{F},\hat{N}])$, for all $\hat{F}\in\partial\hat{T}$ and $\hat{N}\in\hat{F}^*$.

The proposition then follows from Lemma 1 and a theorem of Stenberg [12, Theorem 2.1]. □

For completeness, we reproduce from [12, Theorem 2.1] the theorem from which the above proposition is deduced. Two macroelements are said to be part of an equivalence class $\mathscr{E}$ if they are in correspondence through a mapping g such as defined in (iii) above. A reference macroelement is simply a particular representative in such a class.

DOI: 10.1002/nme

Theorem 3 (*Stenberg*)
Suppose that there is a fixed set of equivalence classes $\mathscr{E}_i$, $i=1,2,\ldots,q$, of macroelements, a positive integer L, and a macroelement partitioning $\mathscr{M}_h$ such that:

1. For each $M \in \mathscr{E}_i$, $i=1,2,\ldots,q$,

$$q_h \in \mathsf{P}_h(M), \int_M q_h \operatorname{div} v_h = 0 \quad \forall v_h \in \mathsf{V}_h^0(M) \;\Rightarrow\; q_h = \text{constant in } M \tag{38}$$

2. Each $M \in \mathscr{M}_h$ belongs to one of the classes $\mathscr{E}_i$, $i=1,\ldots,q$.
3. Each $K \in \mathsf{T}_h$ is contained in at least one and not more than L macroelements of $\mathscr{M}_h$.
4. Each face F of an element of T_h is contained in the interior of at least one and not more than L macroelements of $\mathscr{M}_h$.

Then, the inf–sup condition (37) holds uniformly in h.

Having proved the satisfaction of the inf–sup condition for the couple $\mathsf{V}_h^0 \times \mathsf{P}_h^0$ corresponding to the case $\Gamma_D = \partial\Omega$, we proceed to prove the general result for the couple $\mathsf{V}_h \times \mathsf{P}_h$. Our proof is adapted from [14, p. 181], corresponding to the continuous case. The additional difficulty in the present setting is to ensure the independence of the inf–sup constant from the mesh size. We shall restrict our attention to polyhedral domains and to Dirichlet boundaries of the form: $\Gamma_D = \bigcup_{i=1}^{I} \Gamma_i$, where $\{\Gamma_i,\ i=1,\ldots,I\}$ are faces of Ω.

We begin by recalling the following results from the mathematical theory of mortar methods (see [36–38] or [39, Assumption 4.2, p. 111] for details). Let $\rho^i \in \mathscr{C}_c^\infty(\Gamma_i)$ denote positive smooth functions compactly supported on Γ_i. Assume that the mesh T_h has at least a node inside each Γ_i. Then, there exist functions $\rho_h^i \in \mathsf{V}_h|_{\Gamma_i}$ (more precisely, ρ_h^i are scalar components of functions in V_h, restricted to Γ_i) such that

$$\rho_h^i = 0 \quad \text{on } \partial\Gamma_i \tag{39a}$$

$$\int_{\Gamma_i} \rho_h^i = \int_{\Gamma_i} \rho^i \tag{39b}$$

$$\|\rho_h^i\|_{1/2,00;i} \leqslant C \|\rho^i\|_{1/2,00;i} \tag{39c}$$

where $\|\cdot\|_{1/2,00;i}$ denotes the norm of $H_{00}^{1/2}(\Gamma_i)$ (cf., e.g. [35]). Consider the displacements field $\rho_h^i n_i$ over Γ_i, $i=1,\ldots,I$, where n_i is the *constant* outward unit normal vector on Γ_i. Denote by $\mathscr{R}_h^i(\rho_h^i n_i) \in \mathsf{V}_h$ a classical lifting onto Ω satisfying

$$\mathscr{R}_h^i(\rho_h^i n_i) = \begin{cases} \rho_h^i n_i & \text{on } \Gamma_i \\ 0 & \text{on } \partial\Omega \setminus \Gamma_i \end{cases}$$

and

$$\|\mathscr{R}_h^i(\rho_h^i n_i)\|_{1,\Omega} \leqslant C \|\rho_h^i\|_{1/2,00;i} \tag{40}$$

DOI: 10.1002/nme

We introduce the displacements field

$$w_h = \sum_{i=1}^{I} \mathscr{R}_h^i(\rho_h^i n_i) \tag{41}$$

and consequently, from (40) and (39c),

$$\|w_h\|_{1,\Omega} \leqslant C \sum_{i=1}^{I} \|\rho^i\|_{1/2,00;i} \tag{42}$$

We shall also denote by $\mathscr{P}_h : L^2(\Omega) \to \mathsf{P}_h$ the L^2 orthogonal projection onto P_h, defined by

$$\int_\Omega q_h \mathscr{P}_h p = \int_\Omega q_h p \quad \forall q_h \in \mathsf{P}_h \tag{43}$$

for all $p \in L^2(\Omega)$.

Proposition 2
Let Ω be a polyhedron and assume that the Dirichlet boundary is of the form $\Gamma_D = \bigcup_{i=1}^{I} \Gamma_i$ where $\{\Gamma_i,\ i = 1, \ldots, I\}$ are faces of Ω. Let T_h be a triangulation of Ω and suppose that the interior of every boundary face Γ_i contains at least a node of T_h. Then, there exists a constant $\beta > 0$ independent of the mesh size such that

$$\inf_{q_h \in \mathsf{P}_h \setminus \{0\}} \sup_{v_h \in \mathsf{V}_h \setminus \{0\}} \frac{\int_\Omega q_h \operatorname{div} v_h}{\|q_h\|_{0,\Omega} \|v_h\|_{1,\Omega}} \geqslant \beta \tag{44}$$

Proof
Let $q \in \mathsf{P}_h$ be an arbitrary field of pressure. Let $\lambda_h \in \mathbb{R}$ be such that

$$\lambda_h \left(\sum_{i=1}^{I} \int_{\Gamma_i} \rho^i \right) = \int_\Omega q \tag{45}$$

Define $q_0 \in \mathsf{P}_h$ as

$$q_0 = q - \lambda_h \mathscr{P}_h (\operatorname{div} w_h) \tag{46}$$

Since constant pressures belong to P_h, an application of (43), definition (41) of w_h and integral relation (39b) gives

$$\int_\Omega q_0 = \int_\Omega q - \lambda_h \left(\sum_{i=1}^{I} \int_{\Gamma_i} \rho^i \right) = 0 \tag{47}$$

where the last equality follows from (45). Therefore, we have $q_0 \in \mathsf{P}_h^0$, and Lemma 1 ensures the existence of $v_0 \in \mathsf{V}_h^0$ such that (cf., e.g. [14, Lemma A.42, p. 471])

$$b(v_0, \mu) = \int_\Omega q_0 \mu \quad \forall \mu \in \mathsf{P}_h^0 \tag{48}$$

and

$$\|v_0\|_{1,\Omega} \leqslant \frac{1}{\beta_0} \|q_0\|_{0,\Omega} \tag{49}$$

DOI: 10.1002/nme

Note that equality (48) also holds for any constant pressure μ because $\int_\Omega q_0 = 0$ and $v_0 = 0$ on $\partial\Omega$. Introducing

$$v = v_0 + \lambda_h w_h \tag{50}$$

(48) and (43) give

$$b(v, \mu) = \int_\Omega q\mu \quad \forall \mu \in \mathsf{P}_h \tag{51}$$

Finally, from the definition of v, the stability estimate (49), the definition of q_0 and the estimate (42), we get

$$\begin{aligned} \|v\|_{1,\Omega} &\leqslant \|v_0\|_{1,\Omega} + |\lambda_h| \|w_h\|_{1,\Omega} \\ &\leqslant \frac{1}{\beta_0} \|q_0\|_{0,\Omega} + |\lambda_h| \|w_h\|_{1,\Omega} \leqslant \frac{1}{\beta_0} \|q\|_{0,\Omega} + 2|\lambda_h| \|w_h\|_{1,\Omega} \\ &\leqslant \frac{1}{\beta_0} \|q\|_{0,\Omega} + C|\lambda_h| \end{aligned} \tag{52}$$

where the constant C is independent of the discretization. From (45), Cauchy–Schwarz inequality gives

$$|\lambda_h| \leqslant C \|q\|_{0,\Omega} \tag{53}$$

Hence, it follows from (52) that

$$\|v\|_{1,\Omega} \leqslant C \|q\|_{0,\Omega} \tag{54}$$

The existence of $v \in \mathsf{V}_h$ satisfying (51) and (54) is equivalent to the satisfaction of the inf–sup condition for the pair of spaces $\mathsf{V}_h \times \mathsf{P}_h$, as advertised. □

2.5. Discussion

2.5.1. Crossed triangles. One of the first schemes to exploit a special mesh topology is the crossed-triangle element of Nagtegaal *et al.* [16], further discussed and analysed by Mercier [17] and Kikuchi [18]. The modified approach by Ruas [40] falls within the same category. Specially designed for two-dimensional problems, the scheme consists of splitting quadrilateral elements into four triangles, as shown in Figure 6(a). A standard $\mathbb{P}_1/\mathbb{P}_0$ approximation for displacements and pressures is then used on the resulting triangulation. The aim of the crossed-triangles scheme is to achieve locking-free optimal low-order approximation for square meshes. Indeed, numerical tests show that the scheme performs similarly to the standard non-locking $\mathbb{Q}_1/\mathbb{P}_0$ interpolation. Nevertheless, both the crossed triangles and the $\mathbb{Q}_1/\mathbb{P}_0$ schemes fail to satisfy the inf–sup condition.

In particular, pressure fields obtained by means of crossed triangles exhibit the spurious *checkerboard* mode shown in Figure 6(b), and the pressure field fails to converge in the incompressible limit $\varepsilon \to 0$. However, if the pressure field is constrained to be constant over each quadrilateral element, the inf–sup condition is readily shown to be satisfied, e.g. by the *macroelement* analysis of Boland–Nicolaides [20, 21] and Stenberg [12, 22, 23], as in the proof of Proposition 1.

DOI: 10.1002/nme

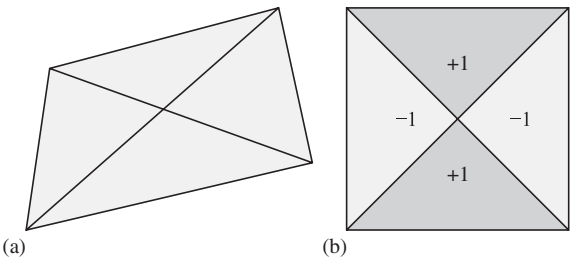

Figure 6. (a) Crossed triangles obtained by splitting a quadrangle and (b) checkerboard mode in crossed triangles.

A common implementation of these ideas is to average the pressure field over each quadrilateral element *a posteriori*. However, it should be carefully noted that *a posteriori* averaging does not eliminate the large local pressure oscillations that arise within each crossed-triangular element. These oscillations eventually cause numerical difficulties due to ill-conditioning.

Crossed triangles supply a familiar example of a scheme that, owing to its failure to satisfy the inf–sup condition, yields divergent pressure fields in the incompressible limit. Additional drawbacks of the approach are the lack of a natural extension to higher-dimensions, and its reliance on quadrilateral meshes, which are often more difficult to generate than triangulations.

2.5.2. Bubble enrichment. A common strategy for alleviating locking is to add bubble functions to the finite element interpolation. A classical example is the MINI $\mathbb{P}_1$-bubble/$\mathbb{P}_1$ element first introduced by Crouzeix and Raviart [4] and subsequently analyzed by Arnold *et al*. [7]. The present scheme may be regarded as consisting of the introduction of piecewise-affine bubble functions, together with an optimal choice of pressure space. It should be carefully noted that pressure interpolation in the MINI $\mathbb{P}_1$-bubble/$\mathbb{P}_1$ scheme is continuous, which renders the incompressibility constraint non-local and requires the use of global pressure degrees of freedom. By contrast, our choice of pressure interpolation is piecewise constant, and the pressure constraint is enforced locally at the element level.

2.5.3. Other special meshes. The topology of two-dimensional diamond meshes bears resemblance to that of special meshes investigated by Le Tallec [19] in connection with the inf–sup condition. However, unlike those meshes studied by Le Tallec, diamond meshes derive from simplicial meshes, which are easier to generate than hexahedral meshes, and are defined in any spatial dimension.

2.5.4. Variations on the diamond theme. Finally, we note that a number of essentially equivalent variations of the diamond concept are possible. A careful inspection of the proof of Proposition 1 reveals that, provided that no additional nodes are added, the precise form of the displacement interpolation within the diamond cells is immaterial as regards convergence. In consequence, variations of the diamond approximation scheme consisting of replacing the bi-simplicial displacement interpolation described in the foregoing by a different displacement interpolation scheme do not alter the approach in any essential way. For instance, each diamond cell could be partitioned into d d-simplices by introducing an edge between the two apices of the cell. Alternatively, a smooth displacement interpolation could be defined in each diamond cell. In either case, the proof of

DOI: 10.1002/nme

Proposition 1 remains essentially unchanged. Thus, the essence of the diamond scheme is largely of a topological nature: diamond cells must be in correspondence with the faces of the initial simplicial mesh; and each diamond cell must carry a constant pressure.

3. DISCRETE MECHANICS RE-INTERPRETATION

Whereas the differential complex that underlies potential theory, electromagnetism and other vector field theories in $\mathbb{R}^3$, namely the classical de Rham complex with its familiar differential operators grad, curl and div, is well-known, the corresponding differential complex underlying *tensor* field theories such as linear elasticity appear to be known to a comparatively lesser degree. The three-dimensional tensor differential complex was fully developed in connection with linear-elastic dislocation theory by Kröner [24] and its differential operators are summarized in Table I. In this table, $\Omega^*(V)$ denotes the graded algebra of C^∞ forms over an open subset of $\mathbb{R}^3$ taking values in a vector space V. The operator Def, or symmetric gradient, applied to a displacement field returns the corresponding strain field. Thus, the equation $\varepsilon = \mathsf{Def}\, u$ represents the classical strain–displacement relations of linear elasticity. The incompatibility operator Inc applied to a symmetric tensor field returns a measure of its incompatibility, i.e. its failure to be a compatible strain field. In particular, if ε is a strain field, then it follows that $\mathsf{Inc}\,\varepsilon = 0$, which are the classical *compatibility equations* of linear elasticity. In general, fields of the form $\mathsf{Inc}\,\varepsilon$ represent a linearization of the curvature tensor associated with the linearized metric ε, and will be referred to as discrete curvature fields. Given a symmetric tensor field σ, $\mathsf{Div}\,\sigma$ represents the net out-of-balance internal force field. In particular, if σ derives from a three-dimensional Airy stress potential A, i.e. if $\sigma = \mathsf{Inc}\, A$, then it follows that σ is in equilibrium, i.e. $\mathsf{Div}\,\sigma = 0$. Thus we have the relations

$$\mathsf{Inc} \circ \mathsf{Def} = 0 \tag{55a}$$

$$\mathsf{Div} \circ \mathsf{Inc} = 0 \tag{55b}$$

In addition, under suitable technical conditions $\ker(\mathsf{Inc}) = \mathrm{im}(\mathsf{Def})$, $\ker(\mathsf{Div}) = \mathrm{im}(\mathsf{Inc})$, and the sequence of vector spaces and operators

$$0 \longrightarrow \Omega^0(\mathbb{R}^3)/\mathsf{RM} \xrightarrow{\mathsf{Def}} \Omega^3(\mathrm{sym}\,\mathbb{R}^{3\times 3}) \xrightarrow{\mathsf{Inc}} \Omega^3(\mathrm{sym}\,\mathbb{R}^{3\times 3}) \xrightarrow{\mathsf{Div}} \Omega^0(\mathbb{R}^3)/\mathsf{RM} \longrightarrow 0 \tag{56}$$

defines an *exact short sequence*, i.e. the range of each map *coincides* with the kernel of the following map [41]. RM denotes the finite-dimensional space of rigid displacements. In terms of

Table I. The tensor Kröner complex in $\mathbb{R}^3$. The first column collects the designation, domain and range of the operators; the second column collects their definition in operator notation; and the third column collects their expression in orthonormal cartesian co-ordinates.

Domain and range	'Nabla' expression	Co-ordinate expression
$\mathsf{Def} : \Omega^0(\mathbb{R}^3) \to \Omega^3(\mathrm{sym}\,\mathbb{R}^{3\times 3})$	$\nabla^S \equiv (\nabla + \nabla^{\mathrm{t}})/2$	$(\mathsf{Def}\, u)_{ij} = (u_{i,j} + u_{j,i})/2$
$\mathsf{Inc} : \Omega^3(\mathrm{sym}\,\mathbb{R}^{3\times 3}) \to \Omega^3(\mathrm{sym}\,\mathbb{R}^{3\times 3})$	$\nabla \times (\bullet \times \nabla)$	$(\mathsf{Inc}\,\varepsilon)_{ij} = \varepsilon_{kl,mn} e_{kmi} e_{lnj}$
$\mathsf{Div} : \Omega^3(\mathrm{sym}\,\mathbb{R}^{3\times 3}) \to \Omega^0(\mathbb{R}^3)$	$\nabla\cdot$	$(\mathsf{Div}\,\sigma)_i = \sigma_{ij,j}$

DOI: 10.1002/nme

tensor differential operators, the boundary-value problem of linear elasticity may be expressed in the form

$$-\mathsf{Div}(\mathbf{C}\,\mathsf{Def}\,u) = f + t \quad \text{in } \Omega \cup \Gamma_{\mathrm{N}} \tag{57a}$$

$$u = 0 \qquad \text{on } \Gamma_{\mathrm{D}} \tag{57b}$$

and the boundary-value problem of incompressible isotropic linear elasticity takes the form

$$-\mathsf{Div}(2\mu\,\mathsf{Def}\,u + p\,g^{\sharp}) = f + t \quad \text{in } \Omega \cup \Gamma_{\mathrm{N}} \tag{58a}$$

$$g^{\sharp} : \mathsf{Def}\,u = 0 \qquad \text{in } \Omega \tag{58b}$$

$$u = 0 \qquad \text{on } \Gamma_{\mathrm{D}} \tag{58c}$$

where Ω is, e.g. an open, simply connected and bounded subset of $\mathbb{R}^d$ with Lipshitz boundary, $\mathbf{C}$ denotes the tensor of elastic moduli, $g^{\sharp}$ is the contravariant metric tensor, respectively, and $g^{\sharp} : \varepsilon$ is the trace of a symmetric tensor ε. Without loss of generality, we restrict attention to homogeneous displacement boundary conditions. In addition, for reasons that will become apparent in the sequel, we have combined the tractions t with the body forces f by regarding both as signed Radon measures with supports on Γ_{N} and Ω, respectively, and interpreting (57a) an (58a) in the sense of measures.

In this section we show that the discrete boundary-value problem of incompressible linear elasticity that results from the diamond approximation scheme can be expressed in terms of a discrete counterpart of the tensor differential complex just described; and that, when expressed in terms of discrete differential operators, the discrete boundary-value problem is formally identical to the classical boundary-value problem (58a)–(58c). The discrete tensor differential complex and its discrete differential operators have properties that are, for the most part, identical to those of the classical tensor differential complex enumerated above. In defining the discrete tensor differential complex, both the *topology* of diamond meshes, regarded as algebraic complexes (e.g. [42]) and their geometry, regarded as an embedding of the algebraic complex in $\mathbb{R}^3$, play a crucial role. This re-interpretation provides compelling new insights into the diamond approximation scheme in terms of geometric and differential structures.

In order to define the discrete operators, we need to adopt a somewhat more expanded view of diamond meshes than required previously for the strict purposes of analysis. In particular, we need a proper accounting of cells of all dimensions, e.g. vertices, edges, faces and volume cells, in the mesh. A natural accounting device for that purpose is to regard meshes as (regular) cell complexes over $\mathbb{R}^d$ (cf., e.g. [42] for relevant definitions and background). The complexes required for the definition of the diamond discrete differential complex are as follows. With reference to Section 2.3, we start by re-interpreting the initial triangulation $\mathscr{T}_h$ of the domain as a simplicial complex. Next, we introduce a finer simplicial complex $\mathscr{S}_h$ obtained by inserting an additional vertex at the barycentre of each d-simplex of $\mathscr{T}_h$ and then subdividing the d-simplices accordingly. Finally, we define the *diamond complex* $\mathscr{D}_h$ as the cell complex whose d-cells are obtained by grouping pairs of d-simplices of $\mathscr{S}_h$ incident on a common $(d-1)$-simplex of $\mathscr{T}_h$.

We shall denote by $E^p(\mathscr{C})$ the set of p-cells of complex $\mathscr{C}$, and by $\Omega^p(\mathscr{C}; V) = \{\omega : E^p(\mathscr{C}) \to V\}$ the space of functions or discrete forms, defined on $E^p(\mathscr{C})$ taking values in the vector space V. We shall use the expressions $F \prec T$ and $T \succ F$ to denote that F is a face of a cell T; $N \prec F$ and

DOI: 10.1002/nme

$F \succ N$ to denote that N is a vertex of the face F; and the symbol $|T|$ to denote the p-dimensional Hausdorff measure of a p-cell T in $\mathbb{R}^d$. We shall also use the symbol n to denote the outward unit normal to a $(d-1)$-cell F. In the remainder of this section, we restrict our attention throughout to the three-dimensional case, $d=3$. Given $\varepsilon \in \mathbb{R}^{3\times 3}$ and $\mathsf{n} \in \mathbb{R}^3$ we shall additionally denote by $\varepsilon \times \mathsf{n} \in \mathbb{R}^{3\times 3}$ the matrix whose rows are the cross-products of the rows of ε and n; and by $\mathsf{n} \times \varepsilon \in \mathbb{R}^{3\times 3}$ the matrix whose columns are the cross-products of n with the columns of ε. Finally, we denote by $\operatorname{sym} \mathbb{R}^{3\times 3}$ the set of symmetric matrices in $\mathbb{R}^{3\times 3}$.

3.1. The simplicial tensor differential complex

Throughout this section $\mathscr{S}_h$ denotes a general simplicial complex.

Definition 1 (*Discrete deformation operator*)
The discrete deformation operator $\mathsf{Def} : \Omega^0(\mathscr{S}_h; \mathbb{R}^3) \to \Omega^3(\mathscr{S}_h; \operatorname{sym} \mathbb{R}^{3\times 3})$ assigns to every discrete displacement field $\mathsf{u} \in \Omega^0(\mathscr{S}_h; \mathbb{R}^3)$ the discrete strain field

$$(\mathsf{Def}\,\mathsf{u})(T) = \frac{1}{2|T|} \sum_{F \prec T} |F|(\langle \mathsf{u} \rangle \otimes \mathsf{n} + \mathsf{n} \otimes \langle \mathsf{u} \rangle) \quad \forall T \in E^3(\mathscr{S}_h) \tag{59}$$

In this expression, $\langle \mathsf{u} \rangle$ denotes the average of the displacements of the vertices of the face F.

Remark 1
Let $I_h \mathsf{u}$ be the piecewise-affine interpolation of the discrete displacements $\mathsf{u} \in \Omega^0(\mathscr{S}_h; \mathbb{R}^3)$ over the tetrahedra $T \in E^3(\mathscr{S}_h)$. Then, it follows from definition (59) that

$$(\mathsf{Def}\,\mathsf{u})(T) = \frac{1}{|T|} \int_T \varepsilon(I_h \mathsf{u}) = \varepsilon(I_h \mathsf{u})_{|T} \quad \forall T \in E^3(\mathscr{S}_h) \tag{60}$$

Thus, the discrete deformation operator yields discrete strain fields that are identical to those computed by direct differentiation of the displacement interpolation.

Definition 2 (*Discrete incompatibility operator*)
The discrete incompatibility operator $\mathsf{Inc} : \Omega^3(\mathscr{S}_h; \operatorname{sym} \mathbb{R}^{3\times 3}) \to \Omega^3(\mathscr{S}_h; \operatorname{sym} \mathbb{R}^{3\times 3})$ assigns to every discrete strain field $\varepsilon \in \Omega^3(\mathscr{S}_h; \operatorname{sym} \mathbb{R}^{3\times 3})$ the discrete curvature field

$$(\mathsf{Inc}\,\varepsilon)(T) = \frac{1}{|T|} \sum_{F \prec T,\ F \not\subset \partial\Omega} (\mathsf{n} \times [\![\varepsilon]\!]) \times \mathsf{n}, \quad \forall T \in E^3(\mathscr{S}_h) \tag{61}$$

where $[\![\varepsilon]\!]$ denotes the jump of ε across F.

Remark 2
A simple computation shows that $(\mathsf{Inc}\,\varepsilon)(T)$ is indeed symmetric for all $T \in E^3(\mathscr{S}_h)$.

We proceed to show that, as is the case for the classical incompatibility operator, the discrete incompatibility operator is self-adjoint.

Lemma 2
The Inc operator is symmetric, i.e. for every $\alpha, \beta \in \Omega^3(\mathscr{S}_h; \operatorname{sym} \mathbb{R}^{3\times 3})$,

$$\sum_{T \in E^3(\mathscr{S}_h)} |T| \mathsf{Inc}(\alpha) : \beta = \sum_{T \in E^3(\mathscr{S}_h)} |T| \mathsf{Inc}(\beta) : \alpha \tag{62}$$

DOI: 10.1002/nme

Proof
The claim easily follows from the identities: $[(n \times B) \times n] \cdot A = B \cdot [n \times (A \times n)]$, $n \in \mathbb{R}^3$, $A,\ B \in \mathbb{R}^{3\times 3}$; and $n \times (A \times n) = (n \times A) \times n$, $n \in \mathbb{R}^3$, $A \in \operatorname{sym} \mathbb{R}^{3\times 3}$. □

Next we proceed to define the discrete differential complex.

Definition 3 (*Discrete divergence operator*)
The discrete divergence operator $\mathsf{Div} : \Omega^3(\mathscr{S}_h; \operatorname{sym} \mathbb{R}^{3\times 3}) \to \Omega^0(\mathscr{S}_h; \mathbb{R}^3)$ assigns to every stress field $\sigma \in \Omega^3(\mathscr{S}_h; \operatorname{sym} \mathbb{R}^{3\times 3})$ the force field

$$(\mathsf{Div}\,\sigma)(N) = \frac{1}{3} \sum_{F \succ N} |F| [\![\sigma]\!] \cdot \mathsf{n} \quad \forall N \in E^0(\mathscr{S}_h) \tag{63}$$

The following lemma shows that the adjointness relations between the classical Def and Div operators carry over to the discrete setting.

Lemma 3
For every $\mathsf{u} \in \Omega^0(\mathscr{S}_h; \mathbb{R}^3)$, $\sigma \in \Omega^3(\mathscr{S}_h; \operatorname{sym} \mathbb{R}^{3\times 3})$, we have

$$\sum_{N \in E^0(\mathscr{S}_h)} (\mathsf{Div}\,\sigma) \cdot \mathsf{u} = - \sum_{T \in E^3(\mathscr{S}_h)} |T| (\mathsf{Def}\,\mathsf{u}) : \sigma \tag{64}$$

where $[\![\sigma]\!]$ denotes the jump of σ across F if F is an interior face; and $-\sigma(T)$ if $F \prec T$ is a boundary face.

Proof
From the definitions of the Def and Div operators, denoting by σ_h the piecewise constant function over Ω such that $(\sigma_h)_{|T} = \sigma(T)$, for all $T \in E^3(\mathscr{S}_h)$ and $\sigma \in \Omega^3(\operatorname{sym} \mathbb{R}^{3\times 3})$, and using the notation $u_h = I_h \mathsf{u}$ from Remark 1, we verify that

$$\begin{aligned}
\sum_{N \in E^0(\mathscr{S}_h)} (\mathsf{Div}\,\sigma) \cdot \mathsf{u} &= - \sum_{T \in E^3(\mathscr{S}_h)} |T| (\mathsf{Def}\,\mathsf{u}) : \sigma \\
&= - \int_\Omega \varepsilon(u_h) : \sigma_h = \int_\Omega u_h \cdot \operatorname{div} \sigma_h + \sum_{F \in E^2(\mathscr{S}_h)} \int_F ([\![\sigma_h]\!] \cdot n) \cdot u_h \\
&= \sum_{F \in E^2(\mathscr{S}_h)} |F| ([\![\sigma]\!] \cdot \mathsf{n}) \cdot \langle \mathsf{u} \rangle = \frac{1}{3} \sum_{F \in E^2(\mathscr{S}_h)} \sum_{N \prec F} |F| ([\![\sigma]\!] \cdot \mathsf{n}) \cdot \mathsf{u}(N) \\
&= \sum_{N \in E^0(\mathscr{S}_h)} \left(\frac{1}{3} \sum_{F \in E^2(\mathscr{S}_h);\ N \in F} |F| [\![\sigma]\!] \cdot \mathsf{n} \right) \cdot \mathsf{u}(N)
\end{aligned}$$

as required. □

Next we show the sequence $\mathsf{Def} \to \mathsf{Inc} \to \mathsf{Div}$ of discrete differential operators defines a differential complex analogous to the classical de Rham complex in $\mathbb{R}^n$.

Lemma 4
$\mathsf{Inc} \circ \mathsf{Def} = 0$ and $\mathsf{Div} \circ \mathsf{Inc} = 0$.

DOI: 10.1002/nme

Table II. The discrete tensor differential complex in $\mathbb{R}^3$. The first column displays the designation, domain and range of the operators; and the second column collects their definitions. In these definitions, $N \in E^0(\mathscr{S}_h)$, $F \in E^2(\mathscr{S}_h)$ and $T \in E^3(\mathscr{S}_h)$.

Domain and range	Definition
$\mathsf{Def} : \Omega^0(\mathscr{S}_h; \mathbb{R}^3) \to \Omega^3(\mathscr{S}_h; \operatorname{sym} \mathbb{R}^{3\times 3})$	$(\mathsf{Def}\,\mathsf{u})(T) = \frac{1}{2\lvert T\rvert}\sum_{F \prec T} \lvert F\rvert(\langle \mathsf{u}\rangle \otimes \mathsf{n} + \mathsf{n} \otimes \langle \mathsf{u}\rangle)$
$\mathsf{Inc} : \Omega^3(\mathscr{S}_h; \operatorname{sym} \mathbb{R}^{3\times 3}) \to \Omega^3(\mathscr{S}_h; \operatorname{sym} \mathbb{R}^{3\times 3})$	$(\mathsf{Inc}\,\varepsilon)(T) = \frac{1}{\lvert T\rvert}\sum_{F \prec T,\ F \not\subset \partial\Omega} (\mathsf{n} \times [\![\varepsilon]\!]) \times \mathsf{n}$
$\mathsf{Div} : \Omega^3(\mathscr{S}_h; \operatorname{sym} \mathbb{R}^{3\times 3}) \to \Omega^0(\mathscr{S}_h; \mathbb{R}^3)$	$(\mathsf{Div}\,\sigma)(N) = \frac{1}{3}\sum_{F \succ N} \lvert F\rvert [\![\sigma]\!] \cdot \mathsf{n}$

Proof

(i) We recall that, for every $T \in E^3(\mathscr{S}_h)$, $(\mathsf{Def}\,\mathsf{u}(T))_{ij} = \frac{1}{2}((\nabla u_h)_{ij} + (\nabla u_h)_{ji})_{|T}$, where $u_h = I_h \mathsf{u}$ is the interpolation of u over $\mathscr{S}_h$. Hence, by the rank-one compatibility of the field ∇u_h we have that $[\![\nabla u_h]\!] = \mathsf{a} \otimes \mathsf{n}$ on every face $F \in \mathscr{S}_h$, whence it follows that

$$(\mathsf{n} \times [\![\mathsf{Def}\,\mathsf{u}]\!]) \times \mathsf{n} = (\mathsf{n} \times [\![\nabla u_h]\!]) \times \mathsf{n} = 0$$

and $\mathsf{Inc} \circ \mathsf{Def} = 0$.

(ii) From the symmetry of $\mathsf{Inc}\,\varepsilon$ for all $\varepsilon \in \operatorname{sym} \mathbb{R}^{3\times 3}$ we have, for every $\mathsf{u} \in \Omega_3(\mathbb{R}^3)$,

$$\begin{aligned}
\sum_{T \in E_3(\mathscr{S}_h)} |T|(\mathsf{Def}\,\mathsf{u}) : (\mathsf{Inc}\,\varepsilon) &= \sum_{T \in E_3(\mathscr{S}_h)} |T|(\nabla u_h) : (\mathsf{Inc}\,\varepsilon) \\
&= \sum_{T \in E_3(\mathscr{S}_h)} \nabla u_h : \sum_{F \prec T,\ F \not\subset \partial\Omega} ((\mathsf{n} \times [\![\varepsilon]\!]) \times \mathsf{n}) \\
&= \sum_{F \in E_2(\mathscr{S}_h),\ F \not\subset \partial\Omega} [\![\nabla u_h]\!] : ((\mathsf{n} \times [\![\varepsilon]\!]) \times \mathsf{n}) \\
&= -\sum_{F \in E_2(\mathscr{S}_h),\ F \not\subset \partial\Omega} ([\![\nabla u_h]\!] \times \mathsf{n}) : (\mathsf{n} \times [\![\varepsilon]\!]) = 0
\end{aligned}$$

and the identity $\mathsf{Div} \circ \mathsf{Inc} = 0$ follows from Lemma 3. □

For ease of reference, we collect the definitions of the discrete tensor differential operators in Table II. The discrete tensor differential operators define the sequence

$$\begin{aligned}
0 \to \Omega^0(\mathscr{S}_h; \mathbb{R}^3)/\mathsf{RM} &\xrightarrow{\mathsf{Def}} \Omega^3(\mathscr{S}_h; \operatorname{sym} \mathbb{R}^{3\times 3}) \xrightarrow{\mathsf{Inc}} \Omega^3(\mathscr{S}_h; \operatorname{sym} \mathbb{R}^{3\times 3}) \\
&\xrightarrow{\mathsf{Div}} \Omega^0(\mathscr{S}_h; \mathbb{R}^3)/\mathsf{RM} \to 0
\end{aligned} \tag{65}$$

From Lemma 4, it follows that each operator has a range included in the kernel of the following operator in the sequence. The conditions under which the sequence is exact are discussed in Section 3.3.

DOI: 10.1002/nme

3.2. The discrete linear elastic boundary-value problem

Without additional structure, the discrete tensor differential complex provides a means of expressing the discrete linear elastic boundary-value problem in a manner that is formally identical to its classical counterpart (57a)–(57b). Here, by the discrete linear elastic boundary-value problem, we specifically mean the Galerkin finite element boundary-value problem for a linear-elastic body discretized by means of a simplicial complex and piecewise-affine displacement interpolation.

We begin by defining the discrete body and surface forces, $\mathsf{f} \in \mathbf{\Omega}^0(\mathscr{S}_h; \mathbb{R}^3)$ and $\mathsf{t} \in \mathbf{\Omega}^0(\mathscr{S}_h; \mathbb{R}^3)$, respectively, as

$$\mathsf{f} = \int_\Omega \phi_N f \quad \forall N \in E^0(\mathscr{S}_h) \tag{66a}$$

$$\mathsf{t} = \begin{cases} \displaystyle\int_{\Gamma_\mathrm{N}} \phi_N t, & N \in E^0(\mathscr{S}_h) \cap \Gamma_\mathrm{N} \\ 0 & \text{elsewhere in } E^0(\mathscr{S}_h) \end{cases} \tag{66b}$$

where ϕ_N denotes the simplicial shape function over $\mathscr{S}_h$ corresponding to node $N \in E^0(\mathscr{S}_h)$. The collection $\{\phi_N, N \in E^0(\mathscr{S}_h)\}$ of all such shape functions defines a basis of V_h. In analogy to the space $H^1_*(\Omega)$ defined in the foregoing, we also introduce the space $\mathbf{\Omega}^0_*(\mathscr{S}_h, \mathbb{R}^3) = \{\mathsf{u} \in \mathbf{\Omega}^0(\mathscr{S}_h, \mathbb{R}^3), \mathsf{u} = \mathsf{0} \text{ on } \Gamma_\mathrm{D}\}$ of discrete displacement fields that satisfy homogeneous displacement boundary conditions identically.

Proposition 3 (*Discrete linear-elastic BVP*)
Let $\mathscr{S}_h$ be a simplicial complex and V_h the corresponding space of piecewise affine interpolants over $\mathscr{S}_h$. Then, the corresponding Galerkin boundary value problem admits the representation

$$-\mathsf{Div}(\mathbf{C}\,\mathsf{Def}\,\mathsf{u}) = \mathsf{f} + \mathsf{t} \quad \text{in } E^0(\mathscr{S}_h)\backslash\Gamma_\mathrm{D} \tag{67a}$$

$$\mathsf{u} = 0 \qquad \text{on } E^0(\mathscr{S}_h) \cap \Gamma_\mathrm{D} \tag{67b}$$

where Def and Div are the discrete deformation and divergence operators over $\mathscr{S}_h$.

Proof
From Lemma 3 and Remark 1 it follows that

$$-\sum_{N \in E^0(\mathscr{S}_h)} (\mathsf{Div}(\mathbf{C}\,\mathsf{Def}\,\mathsf{u})) \cdot \mathsf{v} = \sum_{T \in E^3(\mathscr{S}_h)} |T|(\mathbf{C}\,\mathsf{Def}\,\mathsf{u}) : (\mathsf{Def}\,\mathsf{v}) = a(u_h, v_h) \tag{68}$$

for every $\mathsf{v} \in \mathbf{\Omega}^0(\mathscr{S}_h; \mathbb{R}^3)$, where

$$a(u, v) = \int_\Omega (\mathbf{C}\,\mathsf{Def}\,u) : (\mathsf{Def}\,v) \tag{69}$$

is the Dirichlet bilinear form of anisotropic linear elasticity. In addition, from the definitions (66a) and (66b) we have

$$\sum_{N \in E^0(\mathscr{S}_h)} (\mathsf{f} + \mathsf{t}) \cdot \mathsf{v} = l(v_h) \tag{70}$$

DOI: 10.1002/nme

where $l(v)$ is the external work linear form (2b). The claim then follows from the isomorphism between the spaces $\Omega^0_*(\mathscr{S}_h, \mathbb{R}^3)$ and V_h. □

Lemma 3 also implies that the discrete boundary-value problem (67a)–(67b) has a variational structure, be it in the variational equality form

$$\mathsf{a}(\mathsf{u}, \mathsf{v}) = \mathsf{l}(\mathsf{v}) \quad \forall \mathsf{v} \in \Omega^0_*(\mathscr{S}_h, \mathbb{R}^3) \tag{71}$$

or as the minimum problem

$$\inf_{\mathsf{u} \in \Omega^0_*(\mathscr{S}_h, \mathbb{R}^3)} \mathsf{F}(\mathsf{u}) \tag{72}$$

where

$$\mathsf{a}(\mathsf{u}, \mathsf{v}) = \sum_{T \in E^3(\mathscr{S}_h)} |T| (\mathbf{C}\, \mathsf{Def}\, \mathsf{u}) : (\mathsf{Def}\, \mathsf{v}) \tag{73a}$$

$$\mathsf{l}(\mathsf{u}) = \sum_{N \in E^0(\mathscr{S}_h)} (\mathsf{f} + \mathsf{t}) \cdot \mathsf{u} \tag{73b}$$

$$\mathsf{F}(\mathsf{u}) = \tfrac{1}{2}\mathsf{a}(\mathsf{u}, \mathsf{u}) - \mathsf{l}(\mathsf{u}) \tag{73c}$$

are the discrete Dirichlet bilinear form, the discrete external work linear form and the discrete potential energy, respectively. The proof of Proposition 3 also shows that these variational principles are identical to those obtained by a straight Galerkin reduction of the potential energy.

3.3. The discrete tensor Helmholtz–Hodge decomposition

An example of application of the classical tensor differential complex is the introduction of Airy stress potentials. We proceed to show that the discrete tensor differential complex supplies similar representational tools in the discrete setting. To this end, we begin by establishing the following discrete version of the classical Helmholtz–Hodge decomposition of symmetric tensor fields. This decomposition additionally supplies a powerful connection between tensor-harmonic functions and cohomology analogous to the celebrated de Rahm theorem.

Definition 4 (*Tensor-harmonic functions*)
We say that a symmetric tensor field $\gamma \in \Omega^3(\mathscr{S}_h; \operatorname{sym} \mathbb{R}^{3\times 3})$ is *tensor-harmonic* if $\mathsf{Div}\, \gamma = 0$ and $\mathsf{Inc}\, \gamma = 0$. We shall denote by $\Gamma(\mathscr{S}_h)$ the vector space of tensor-harmonic functions over $\mathscr{S}_h$.

Definition 5 (*Tensor-cohomology groups*)
The groups:

$$H^1(\mathscr{S}_h) = \ker(\mathsf{Def}) \tag{74a}$$

$$H^2(\mathscr{S}_h) = \ker(\mathsf{Inc})/\operatorname{im}(\mathsf{Def}) \tag{74b}$$

$$H^3(\mathscr{S}_h) = \ker(\mathsf{Div})/\operatorname{im}(\mathsf{Inc}) \tag{74c}$$

DOI: 10.1002/nme

are the first, second and third tensor-cohomology groups of $\mathscr{S}_h$, respectively. In these definitions, the discrete operator Def has the domain of definition indicated on the sequence (65).

We introduce the weighted ℓ^2 inner product over $\Omega^3(\mathscr{S}_h; \operatorname{sym}\mathbb{R}^{3\times 3})$

$$\langle \alpha, \beta \rangle = \sum_{T\in E^3(\mathscr{S}_h)} |T|\alpha : \beta \tag{75}$$

We additionally denote by $\ker(T)$ and $\operatorname{im}(T)$ the null and image spaces of a linear operator T, respectively.

Lemma 5 (*Discrete tensor Helmholtz–Hodge decomposition*)
Let $\sigma \in \Omega^3(\mathscr{S}_h; \operatorname{sym}\mathbb{R}^{3\times 3})$ be a symmetric tensor field over $\mathscr{S}_h$. Then

(i) There exit fields $\mathsf{v} \in \Omega^0(\mathscr{S}_h; \mathbb{R}^3)$, $\mathsf{A} \in \Omega^3(\mathscr{S}_h; \operatorname{sym}\mathbb{R}^{3\times 3})$ satisfying the gage condition

$$\mathsf{Div}\,\mathsf{A} = \mathsf{0} \tag{76}$$

and $\gamma \in \Gamma(\mathscr{S}_h)$ such that

$$\sigma = \mathsf{Def}\,\mathsf{v} + \mathsf{Inc}\,\mathsf{A} + \gamma \tag{77}$$

(ii) All the terms of the decomposition are ℓ^2-orthogonal in the sense of the inner product (75).
(iii) The space $\Gamma(\mathscr{S}_h)$ of tensor-harmonic functions is isomorphic to the cohomology group $H^3(\mathscr{S}_h) = \ker(\mathsf{Div})/\operatorname{im}(\mathsf{Inc})$.

Proof
The proof parallels closely the proof of the classical Helmholtz–Hodge decomposition (cf., e.g. [43]). Begin by introducing the bilinear form over $\Omega^3(\mathscr{S}_h; \operatorname{sym}\mathbb{R}^{3\times 3})$

$$(\alpha, \beta) = \langle \mathsf{Div}\,\alpha, \mathsf{Div}\,\beta \rangle + \langle \mathsf{Inc}\,\alpha, \mathsf{Inc}\,\beta \rangle \tag{78}$$

$(\bullet, \bullet)$ is clearly symmetric and strictly positive definite when restricted to the quotient space $\Omega^3(\mathscr{S}_h; \operatorname{sym}\mathbb{R}^{3\times 3})/\Gamma(\mathscr{S}_h)$. Note that for every $\sigma \in \Omega^3(\mathscr{S}_h; \operatorname{sym}\mathbb{R}^{3\times 3})$ we have the orthogonal decomposition

$$\sigma = \gamma + \sigma' \tag{79}$$

with $\gamma \in \Gamma(\mathscr{S}_h)$ and $\langle \gamma, \sigma' \rangle = 0$. Since $(\bullet, \bullet)$ is an inner product on $\Omega^3(\mathscr{S}_h; \operatorname{sym}\mathbb{R}^{3\times 3})/\Gamma(\mathscr{S}_h)$, it follows from the Riesz representation theorem that there exists a unique $\beta \in \Omega^3(\mathscr{S}_h; \operatorname{sym}\mathbb{R}^{3\times 3})/\Gamma(\mathscr{S}_h)$ such that

$$(\beta, \alpha) = \langle \sigma', \alpha \rangle \quad \forall \alpha \in \Omega^3(\mathscr{S}_h; \operatorname{sym}\mathbb{R}^{3\times 3}) \tag{80}$$

From Definition 3 and Lemma 2 it follows that

$$-\sum_{T\in E^3(\mathscr{S}_h)} |T|(\mathsf{Def}\circ\mathsf{Div}\,\beta) : \alpha + \sum_{T\in E^3(\mathscr{S}_h)} |T|(\mathsf{Inc}\circ\mathsf{Inc}\,\beta) : \alpha = \langle \alpha, \sigma' \rangle \tag{81}$$

for every $\alpha \in \Omega^3(\mathscr{S}_h; \operatorname{sym}\mathbb{R}^{3\times 3})$. Setting $\mathsf{v} = -\mathsf{Div}\,\beta$ and $\mathsf{A} = \mathsf{Inc}\,\beta$ we have

$$\mathsf{Div}\,\mathsf{A} = \mathsf{Div}\circ\mathsf{Inc}\,\beta = \mathsf{0} \tag{82a}$$

$$\sigma = \mathsf{Def}\,\mathsf{v} + \mathsf{Inc}\,\mathsf{A} + \gamma \tag{82b}$$

DOI: 10.1002/nme

The orthogonality of the decomposition follows directly from Definition 3, Lemma 4 and the definition of $\Gamma(\mathscr{S}_h)$. Finally, we prove (iii) by showing the canonical projection $\pi : \Gamma(\mathscr{S}_h) \to H^3(\mathscr{S}_h) = \ker(\mathsf{Div})/\mathrm{im}(\mathsf{Inc})$ is one-to-one. Let $\gamma \in \Gamma(\mathscr{S}_h)$ be such that $\pi\gamma = \dot{\mathsf{0}}$, namely, the equivalence class of $\mathsf{0}$ in $H^3(\mathscr{S}_h)$. It follows that there exists $\mathsf{A} \in \Omega^3(\mathscr{S}_h; \mathrm{sym}\,\mathbb{R}^{3\times 3})$ such that $\gamma = \mathsf{Inc}\, A$. Because $\gamma \in \Gamma(\mathscr{S}_h)$, we also have $\mathsf{Inc}\,\gamma = \mathsf{0}$ and, therefore,

$$0 = \langle \mathsf{Inc}\,\gamma, \mathsf{A} \rangle = \langle \gamma, \mathsf{Inc}\,\mathsf{A} \rangle = \langle \gamma, \gamma \rangle \tag{83}$$

Hence $\gamma = \mathsf{0}$ and the injectivity of π follows. To prove surjectivity, let $\dot{\sigma} \in H^3(\mathscr{S}_h)$. Applying the Helmholtz–Hodge decomposition to a representative σ of $\dot{\sigma}$, it follows that there exist $\mathsf{v} \in \Omega^0(\mathscr{S}_h; \mathbb{R}^3)$, $\mathsf{A} \in \Omega^3(\mathscr{S}_h; \mathrm{sym}\,\mathbb{R}^{3\times 3})$ and $\gamma \in \Gamma(\mathscr{S}_h)$, such that

$$\sigma = \mathsf{Def}\,\mathsf{v} + \mathsf{Inc}\,\mathsf{A} + \gamma \tag{84}$$

Since $\mathsf{Div}\,\sigma = \mathsf{0}$, it follows that $\mathsf{Div} \circ \mathsf{Def}\,\mathsf{v} = \mathsf{0}$, hence $0 = \langle \mathsf{v}, \mathsf{Div} \circ \mathsf{Def}\,\mathsf{v} \rangle = \langle \mathsf{Def}\,\mathsf{v}, \mathsf{Def}\,\mathsf{v} \rangle$ and $\mathsf{Def}\,\mathsf{v} = \mathsf{0}$. Consequently, there exists a $\gamma \in \Gamma(\mathscr{S}_h)$ such that $\pi\gamma \in \dot{\sigma}$. □

If the vector space $\Gamma(\mathscr{S}_h)$ of tensor-harmonic functions over $\mathscr{S}_h$ is reduced to $\{0\}$, it follows from Lemmata 5 and 4 that the sequence of discrete tensor differential operators

$$\begin{aligned} 0 \to \Omega^0(\mathscr{S}_h; \mathbb{R}^3)/\mathsf{RM} &\xrightarrow{\mathsf{Def}} \Omega^3(\mathscr{S}_h; \mathrm{sym}\,\mathbb{R}^{3\times 3}) \xrightarrow{\mathsf{Inc}} \Omega^3(\mathscr{S}_h; \mathrm{sym}\,\mathbb{R}^{3\times 3}) \\ &\xrightarrow{\mathsf{Div}} \Omega^0(\mathscr{S}_h; \mathbb{R}^3)/\mathsf{RM} \to 0 \end{aligned} \tag{85}$$

is an exact short sequence. The analogy between the discrete operators and their classical counterparts displayed in Table I is both striking and compelling.

The displacement–strain relations $\varepsilon = \mathsf{Def}\,u$ may be regarded as a special case of the tensor Helmholtz–Hodge decomposition in which the displacement field plays the role of vector potential. Another common application is the representation of a general self-equilibrated stress field σ in terms of a three-dimensional discrete Airy potential A. Thus, if the discrete cohomology group $H^3(\mathscr{S}_h)$ is trivial, i.e., if $\ker(\mathsf{Div}) = \mathrm{im}(\mathsf{Inc})$, then any equilibrated discrete stress field is in $\mathrm{im}(\mathsf{Inc})$ and, therefore, it can be expressed as

$$\sigma = \mathsf{Inc}\,\mathsf{A} \tag{86}$$

Clearly, A is determined up to a discrete deformation, i.e. if A is a potential for σ, then so is $\mathsf{A} + \mathsf{Def}\,\mathsf{u}$, for any $\mathsf{u} \in \Omega^0(\mathscr{S}_h; \mathbb{R}^3)$. In order to resolve this indeterminacy we may append the gage condition

$$\mathsf{Div}\,\mathsf{A} = 0 \tag{87}$$

Then, A is determined up to a tensor-harmonic function and, therefore, is uniquely determined if $H^3(\mathscr{S}_h)$ is trivial. The compatibility condition

$$\mathsf{Inc}(\mathbf{C}^{-1}\sigma) = 0 \tag{88}$$

supplies a discrete analogue of the classical Beltrami–Mitchell compatibility equations (cf., e.g. [44]). The combination of the preceding equations gives

$$\mathsf{Inc}(\mathbf{C}^{-1}\mathsf{Inc}\,\mathsf{A}) = 0 \tag{89}$$

DOI: 10.1002/nme

which, in conjunction with the gage condition (87), supplies a discrete tensor bi-laplacian equation for the Airy potential. As in the classical case, the discrete tensor Helmholtz–Hodge Lemma 5 also establishes a powerful connection between tensor-cohomology and tensor-harmonic functions.

3.4. The discrete metric

The role played by the metric in defining the linear elasticity boundary-value problem is clearly evident in Equations (58a) and (58b). In this section we proceed to define a discrete metric that, as we shall see, plays an analogous role in the formulation of the discrete problem. Whereas the discrete tensor differential complex introduced in the preceding section can be defined on an arbitrary simplicial complex, the definition of the metric makes use of the diamond complex as well. The need for this additional complex is not evident from a purely geometrical and formal point of view, but instead is evidenced by the analysis of convergence in the incompressible limit. In particular, the metric is designed to ensure the satisfaction of the inf–sup condition.

Definition 6 (*Discrete metric*)
Let $g^\sharp$ be the contravariant metric in $\mathbb{R}^3$. Then, the discrete contravariant metric is the constant symmetric field $\mathsf{g}^\sharp \in \Omega^3(\mathscr{D}_h; \operatorname{sym} \mathbb{R}^{3\times 3})$ such that $\mathsf{g}^\sharp(D) = g^\sharp$ for every $D \in E^3(\mathscr{D}_h)$.

Definition 7 (*Trace*)
Let $\varepsilon \in \Omega^3(\mathscr{S}_h; \mathbb{R}^{3\times 3})$ be a discrete symmetric tensor field. Then we define its trace $\mathsf{g}^\sharp : \varepsilon \in \Omega^3(\mathscr{D}_h; \mathbb{R})$ as

$$(\mathsf{g}^\sharp : \varepsilon)(D) = \frac{1}{|D|} \sum_{T \in E^3(\mathscr{S}_h),\ T \subset D} |T| g^\sharp : \varepsilon \quad \forall D \in E^3(\mathscr{D}_h) \tag{90}$$

The precise manner in which the contravariant metric $\mathsf{g}^\sharp$ determines the trace of a symmetric tensor field on the subdivision complex should be carefully noted. Thus, a key part of the computation of the trace consists of *averaging* the field over each three cell in the diamond complex. The result is a scalar field defined on the diamond complex. As shown earlier, the averaging over diamond cells has the far-reaching consequence of ensuring the satisfaction of the inf–sup condition.

Definition 8 (*Isotropic tensors*)
Let $\mathsf{p} \in \Omega^3(\mathscr{D}_h; \mathbb{R})$ be a scalar field. The corresponding isotropic tensor field $\mathsf{p}\,\mathsf{g}^\sharp \in \Omega^3(\mathscr{S}_h; \operatorname{sym} \mathbb{R}^{3\times 3})$ is

$$(\mathsf{p}\,\mathsf{g}^\sharp)(T) = \mathsf{p}(D)\, g^\sharp, \quad T \subset D \tag{91}$$

For instance, if p is a pressure field over the diamond complex, then $\mathsf{p}\,\mathsf{g}^\sharp$ is the corresponding hydrostatic stress field. The following reciprocity relation follows directly from the preceding definitions.

Lemma 6
For every $\varepsilon \in \Omega^3(\mathscr{S}_h; \operatorname{sym} \mathbb{R}^{3\times 3})$ and every $\mathsf{p} \in \Omega^3(\mathscr{D}_h; \mathbb{R})$,

$$\sum_{D \in E^3(\mathscr{D}_h)} |D| \mathsf{p}(\mathsf{g}^\sharp : \varepsilon) = \sum_{T \in E^3(\mathscr{S}_h)} |T| (\mathsf{p}\,\mathsf{g}^\sharp) : \varepsilon \tag{92}$$

DOI: 10.1002/nme

Remark 3
Let $u_h = I_h \mathsf{u}$ be the piecewise-affine interpolation of the discrete displacements $\mathsf{u} \in \Omega^0(\mathscr{S}_h; \mathbb{R}^3)$ over the tetrahedra $T \in E^3(\mathscr{S}_h)$. Then, it follows from definition (6) that

$$\mathsf{g}^\sharp : (\mathsf{Def}\,\mathsf{u})(D) = \frac{1}{|D|} \int_{\mathrm{D}} \operatorname{div} u_h \quad \forall D \in E^3(\mathscr{D}_h) \tag{93}$$

Thus, the trace of the deformation field equals the average divergence of the displacement field on every diamond cell.

3.5. The isotropic discrete differential complex

We recall the classical identities

$$\operatorname{grad} p = \operatorname{div}(p\, g^\sharp) \tag{94a}$$

$$\operatorname{div} u = g^\sharp : \varepsilon(u) \tag{94b}$$

that re-interpret the restriction of the tensor-divergence operator to isotropic fields as a vector-gradient operator, and the trace of the deformation operator as a vector-divergence operator. These operators define the sequence

$$\Omega^0(\mathbb{R}^3) \xrightarrow{\operatorname{div}} \Omega^3(\mathbb{R}) \xrightarrow{0} \Omega^3(\mathbb{R}) \xrightarrow{\operatorname{grad}} \Omega^0(\mathbb{R}^3) \tag{95}$$

The null operator $0 : \Omega^3(\mathbb{R}) \to \Omega^3(\mathbb{R})$ simply reflects the fact that any scalar field in $\Omega^3(\mathbb{R})$ can be expressed as a divergence and, hence, is not subject to any compatibility conditions. We shall refer to this complex as the *isotropic* differential complex in order to emphasize that it is not a vector-differential complex but rather the restriction of the tensor-differential complex to isotropic tensor fields. The corresponding isotropic cohomology groups are $H^2 = \Omega^3(\mathbb{R})/\mathrm{im}(\mathrm{div}) = \{0\}$; $H^3 = \ker(\mathrm{grad})/\mathrm{im}(0) = \ker(\mathrm{grad}) = \mathbb{R}$. In particular, we note that $H^3 = \mathbb{R}$, i.e. if a scalar field has a vanishing gradient then it must necessarily be a constant.

The corresponding discrete differential operators are

$$\mathsf{grad}\,\mathsf{p} = \mathsf{Div}(\mathsf{p}\,\mathsf{g}^\sharp) \tag{96a}$$

$$\mathsf{div}\,\mathsf{u} = \mathsf{g}^\sharp : \mathsf{Def}\,\mathsf{u} \tag{96b}$$

We note the following adjointness relation between grad and div.

Lemma 7
For every $\mathsf{u} \in \Omega^0(\mathscr{S}_h; \mathbb{R}^3)$, $\mathsf{p} \in \Omega^3(\mathscr{D}_h; \mathbb{R})$, we have

$$\sum_{N \in E^0(\mathscr{S}_h)} (\mathsf{grad}\,\mathsf{p}) \cdot \mathsf{u} = -\sum_{D \in E^3(\mathscr{D}_h)} |D| \mathsf{p}\,(\mathsf{div}\,\mathsf{u}) \tag{97}$$

Proof
From Lemma 6 we have

$$\sum_{T \in E^3(\mathscr{S}_h)} |T|(\mathsf{p}\,\mathsf{g}^\sharp) : \mathsf{Def}\,\mathsf{u} = \sum_{D \in E^3(\mathscr{D}_h)} |D| \mathsf{p}(\mathsf{g}^\sharp : \mathsf{Def}\,\mathsf{u}) = \sum_{D \in E^3(\mathscr{D}_h)} |D| \mathsf{p}\,\mathsf{div}\,\mathsf{u} \tag{98}$$

DOI: 10.1002/nme

and from Lemma 3 it follows that

$$\sum_{T\in E^3(\mathscr{S}_h)} |T|(\mathsf{p}\,\mathsf{g}^\sharp) : \mathsf{Def}\,\mathsf{u} = -\sum_{N\in E^0(\mathscr{S}_h)} \mathsf{Div}(\mathsf{p}\,\mathsf{g}^\sharp)\cdot\mathsf{u} = -\sum_{N\in E^0(\mathscr{S}_h)} (\mathsf{grad}\,\mathsf{p})\cdot\mathsf{u} \tag{99}$$

whence (97) follows as required. □

These operators define the sequence

$$\Omega^0_*(\mathscr{D}_h;\mathbb{R}^3) \xrightarrow{\mathsf{div}} \Omega^3_*(\mathscr{D}_h;\mathbb{R}) \xrightarrow{0} \Omega^3_*(\mathscr{D}_h;\mathbb{R}) \xrightarrow{\mathsf{grad}} \Omega^0_*(\mathscr{D}_h;\mathbb{R}^3) \tag{100}$$

where, as before, $\Omega^0_*(\mathscr{D}_h;\mathbb{R}^3)$ denotes the subset of functions in $\Omega^0(\mathscr{D}_h;\mathbb{R}^3)$ vanishing on Γ_D; $\Omega^3_*(\mathscr{D}_h;\mathbb{R})$ stands for the quotient group $\Omega^3(\mathscr{D}_h;\mathbb{R})/\mathsf{S}$, where $\mathsf{S}=\mathbb{R}$ if $\Gamma_D=\partial\Omega$, $\mathsf{S}=\{0\}$ otherwise. By the last arrow in sequence (100) we specifically mean that only the values of the gradient outside Γ_D are considered.

We can also define discrete isotropic cohomology classes as follows.

Definition 9 (*Discrete isotropic cohomology groups*)
The groups:

$$H^2(\mathscr{D}_h) = \Omega^3_*(\mathscr{D}_h;\mathbb{R})/\mathrm{im}(\mathsf{div}) \tag{101a}$$

$$H^3(\mathscr{D}_h) = \ker(\mathsf{grad}) \tag{101b}$$

are the second and third isotropic cohomology groups of $\mathscr{D}_h$, respectively. In this definition, the discrete operators div and grad have the domains of definition indicated in the sequence (100). In addition, by the last arrow in the sequence (100) we specifically mean that only the values of the gradient outside Γ_D are considered.

Naturally, we would like $H^2(\mathscr{D}_h)=\{0\}$, and $H^3(\mathscr{D}_h)=\{0\}$. Remarkably, this condition is equivalent to the inf–sup condition for incompressible linear elasticity. This connection confirms the intuition that the inf–sup condition is largely topological in nature.

Proposition 4
The following statements are equivalent:

(i) $H^2(\mathscr{D}_h)=\{0\}$;
(ii) $H^3(\mathscr{D}_h)=\{0\}$;
(iii) the inf–sup condition (21) is satisfied.

Proof
Begin by recalling the definition: $\mathscr{B}_h : v_h\in\mathsf{V}_h\to\mathsf{P}'_h \ni b(v_h,\cdot)$, where P'_h is the dual of P_h. Condition (21) is classically equivalent to $\ker(\mathscr{B}^t_h)=\{0\}$. By the isomorphism between the spaces $\Omega^0_*(\mathscr{S}_h,\mathbb{R}^3)$ and V_h, $\Omega^3(\mathscr{D}_h,\mathbb{R})$ and P_h, and the definition of grad, this is exactly equivalent to $\ker(\mathsf{grad})=\{0\}$ which means $H^3(\mathscr{D}_h)=\{0\}$. On the other hand, $\ker(\mathsf{grad})=\{0\}$ is equivalent to $\mathrm{im}(\mathsf{div})=\{0\}^\perp=\Omega^3_*(\mathscr{D}_h;\mathbb{R})$. □

Since we have previously shown that the inf–sup condition is satisfied by the diamond approximation scheme, it follows that sequence (100) is indeed exact.

DOI: 10.1002/nme

3.6. The discrete incompressible linear elastic boundary-value problem

The definition of a discrete diamond metric finally provides sufficient structure to define a discrete form of boundary-value problem for incompressible linear elasticity.

Proposition 5 (*Discrete incompressible linear-elastic BVP*)
Let $\mathscr{T}_h$ be a simplicial complex, $\mathscr{S}_h$ its diamond subdivision complex, $\mathscr{D}_h$ its diamond complex. Then, the corresponding Galerkin boundary-value problem admits the representation

$$-\mathsf{Div}(2\mu\,\mathsf{Def}\,\mathsf{u} + \mathsf{p}\,\mathsf{g}^\sharp) = f + t \quad \text{in } E^0(\mathscr{S}_h)\backslash\Gamma_\mathrm{D} \tag{102a}$$

$$\mathsf{g}^\sharp : \mathsf{Def}\,\mathsf{u} = 0 \qquad \text{in } E^3(\mathscr{D}_h) \tag{102b}$$

$$\mathsf{u} = 0 \qquad \text{on } E^0(\mathscr{S}_h) \cap \Gamma_\mathrm{D} \tag{102c}$$

where Def and Div are the discrete deformation and divergence operators over $\mathscr{S}_h$ and $\mathsf{g}^\sharp$ is the discrete contravariant metric over $\mathscr{D}_h$.

Proof
From Lemma 3 and Remark 1 it follows that

$$-\sum_{N\in E^0(\mathscr{S}_h)} (\mathsf{Div}\,(2\mu\,\mathsf{Def}\,\mathsf{u}))\cdot\mathsf{v} = \sum_{T\in E^3(\mathscr{S}_h)} |T|\,2\mu(\mathsf{Def}\,\mathsf{u}) : (\mathsf{Def}\,\mathsf{v}) = a(u_h, v_h) \tag{103}$$

for every $\mathsf{v}\in\Omega^0(\mathscr{S}_h;\mathbb{R}^3)$, where $a(u, v)$ is the isotropic Dirichlet bilinear form (2a). Additionally, from Lemmas 3 and 6 and Remarks 1 and 3 we have

$$\begin{aligned}-\sum_{N\in E^0(\mathscr{S}_h)} (\mathsf{Div}\,(\mathsf{p}\,\mathsf{g}^\sharp))\cdot\mathsf{v} = \sum_{T\in E^3(\mathscr{S}_h)} |T|(\mathsf{p}\,\mathsf{g}^\sharp) : \mathsf{Def}\,\mathsf{v} = \sum_{D\in E^3(\mathscr{D}_h)} |D|\mathsf{p}(\mathsf{g}^\sharp : \mathsf{Def}\,\mathsf{v})\\ = \int_\Omega q_h \,\mathrm{div}\, v_h = b(v_h, q_h)\end{aligned} \tag{104}$$

where the bilinear form $b(\bullet,\bullet)$ is defined in (8a). The claim then follows from (70) and the isomorphism between $\Omega^0_*(\mathscr{S}_h,\mathbb{R}^3)$ and the space V_h of piecewise affine interpolants over $\mathscr{S}_h$, and between $\Omega^3(\mathscr{D}_h,\mathbb{R})$ and the space P_h of piecewise constant interpolants over $\mathscr{D}_h$. □

As in the case of unconstrained linear elasticity, Lemmas 3 and 6 additionally imply that the discrete boundary-value problem (102a)–(102b) has the variational structure

$$\mathsf{a}(\mathsf{u},\mathsf{v}) + \mathsf{b}(\mathsf{v},\mathsf{p}) = \mathsf{l}(\mathsf{v}) \quad \forall\mathsf{v}\in\Omega^0_*(\mathscr{S}_h,\mathbb{R}^3) \tag{105a}$$

$$\mathsf{b}(\mathsf{u},\mathsf{q}) = 0 \qquad \forall\mathsf{q}\in\Omega^3(\mathscr{D}_h,\mathbb{R}) \tag{105b}$$

where

$$\mathsf{a}(\mathsf{u},\mathsf{v}) = \sum_{T\in E^3(\mathscr{S}_h)} |T|2\mu\,(\mathsf{Def}\,\mathsf{u}) : (\mathsf{Def}\,\mathsf{v}) \tag{106a}$$

DOI: 10.1002/nme

$$\mathsf{b}(\mathsf{u},\mathsf{p}) = \sum_{D\in E^3(\mathscr{D}_h)} |D|\mathsf{p}(\mathsf{g}^\sharp : \mathsf{Def}\,\mathsf{u}) \tag{106b}$$

are the discrete Dirichlet bilinear form and the bilinear form corresponding to the incompressibility constraint, respectively. The proof of Proposition 5 also shows that the discrete variational problem is identical to the diamond discrete boundary-value problem obtained by mixed interpolation of displacement and pressures. Proposition 4 then provides a purely topological means of verifying the inf–sup condition through the computation of the discrete isotropic cohomology group $H^3(\mathsf{D}_h)$.

4. NUMERICAL EXAMPLES

4.1. Non-linear elasticity

In this section, we proceed to formally extend the diamond approach to finite-deformation elasticity and assess its performance in selected benchmark problems. Whereas, as shown in the foregoing, the case of linearized elasticity is amenable to analysis, comparable analysis tools for finite deformation problems are lacking at present. Therefore, the present discussion is limited to issues of implementation and to demonstrating scope and performance by way of numerical experiment.

For definiteness, we consider an incompressible elastic material with a free energy of neo-Hookean type, namely

$$W = W^{\mathrm{dev}}(\boldsymbol{F}^{\mathrm{dev}}) + W^{\mathrm{vol}}(J^*) \tag{107}$$

Conveniently, this energy density can be additively decomposed into a deviatoric part:

$$W^{\mathrm{dev}} = \tfrac{1}{2}\mu[\boldsymbol{F}^{\mathrm{dev}} : \boldsymbol{F}^{\mathrm{dev}} - d] \tag{108}$$

and a volumetric part:

$$W^{\mathrm{vol}}(J^*) = \tfrac{1}{2}\kappa[J^* - 1]^2 \tag{109}$$

In these expressions, the deviatoric part of the deformation gradient is defined as

$$\boldsymbol{F}^{\mathrm{dev}} = J^{-1/d}\boldsymbol{F} \tag{110}$$

where

$$J = \det(\boldsymbol{F}) \tag{111}$$

is the Jacobian of the deformation and d denotes the spatial dimension. The notational convention of denoting the volumetric deformation by J^* is designed to emphasize that the volumetric deformation is not necessarily evaluated at the same location as the deformation gradient $\boldsymbol{F}$. The total free energy of the quasi-incompressible elastic material is, therefore,

$$W = \tfrac{1}{2}\mu J^{-2/d}[\boldsymbol{F} : \boldsymbol{F} - d] + \tfrac{1}{2}\kappa[J^* - 1]^2 \tag{112}$$

and the first Piola Kirchhoff stress $\boldsymbol{P} = \mathrm{d}_{\boldsymbol{F}} W$ follows in the form

$$\boldsymbol{P} = \mu J^{-2/d}[\,\boldsymbol{F} - \tfrac{1}{d}[\boldsymbol{F} : \boldsymbol{F}]\boldsymbol{F}^{-\mathrm{t}}] + J\kappa[J^* - 1]\boldsymbol{F}^{-\mathrm{t}} \tag{113}$$

DOI: 10.1002/nme

In particular, the hydrostatic pressure $p = \mathrm{tr}(J^{-1}\boldsymbol{P}\boldsymbol{F}^{\mathrm{T}})/d$ is computed to be

$$p = -\kappa[J^* - 1] \tag{114}$$

and, hence, we can interpret κ as a penalty parameter that enforces the incompressibility constraint

$$J^* - 1 \doteq 0 \tag{115}$$

The linearization of the first Piola Kirchhoff stress $\boldsymbol{P}$ with respect to the deformation gradient $\boldsymbol{F}$ yields the tangent moduli

$$\begin{aligned}\mathbf{A} = {} & \frac{2}{dF^2}\mu J^{-2/d}[\boldsymbol{F}:\boldsymbol{F}][\boldsymbol{F}^{-\mathrm{t}}\otimes\boldsymbol{F}^{-\mathrm{t}}] + \frac{1}{d}\mu J^{-2/d}[\boldsymbol{F}:\boldsymbol{F}][\boldsymbol{F}^{-\mathrm{t}}\underline{\otimes}\boldsymbol{F}^{-1}] \\ & -\frac{2}{d}\mu J^{-2/d}[\boldsymbol{F}\otimes\boldsymbol{F}^{-\mathrm{t}} + \boldsymbol{F}^{-\mathrm{t}}\otimes\boldsymbol{F}] + \mu J^{-2/d}\boldsymbol{I}\overline{\otimes}\boldsymbol{I} \\ & +J\kappa[J^* - 1][\boldsymbol{F}^{-\mathrm{t}}\otimes\boldsymbol{F}^{-\mathrm{t}} - \boldsymbol{F}^{-\mathrm{t}}\underline{\otimes}\boldsymbol{F}^{-1}] + J\kappa[\boldsymbol{F}^{-\mathrm{t}}\otimes\partial_{\boldsymbol{F}}J^*]\end{aligned} \tag{116}$$

which are of fundamental importance for the numerical solution procedure. The non-standard dyadic products introduced in (116) are defined *via* the identities: $[\boldsymbol{A}\overline{\otimes}\boldsymbol{B}]\cdot\boldsymbol{C} = \boldsymbol{A}\cdot\boldsymbol{C}\cdot\boldsymbol{B}^{\mathrm{t}}$ and $[\boldsymbol{A}\underline{\otimes}\boldsymbol{B}]\cdot\boldsymbol{C} = \boldsymbol{A}\cdot\boldsymbol{C}^{\mathrm{t}}\cdot\boldsymbol{B}^{\mathrm{t}}$, in terms of the second-order tensors $\boldsymbol{A}$, $\boldsymbol{B}$ and $\boldsymbol{C}$.

4.2. Element types

In two dimensions we evaluate the performance of five different lower-order elements. By way of baseline we consider the standard linear triangle `P1` and the standard linear quadrilateral `Q1`. The third element is denoted as `4P1P0`, also referred to as `4CST` element in the specialized literature. It is composed of four crossed constant-strain triangles and was originally proposed by Nagtegaal *et al*. [16]. In order to eliminate local pressure oscillations, we plot the averaged pressure on each four-triangle patch as suggested, e.g. by Kikuchi [18]. Finally, we consider the `2P1P0` F-bar element of De Souza Neto *et al.* [45], consisting of a patch of two triangles with and constant pressure which can be understood as a geometrically non-linear generalization of the element introduced by Ruas [40]; and the F-bar quadrilateral `Q1P0` of Moran *et al.* [46]. These five elements are depicted in Figure 7, with white circles denoting displacement nodes and the dark circles denoting pressure nodes. For each type of element, we analyse two different mesh geometries. The first geometry consists of regular square meshes built from the elements just enumerated and shown in Figure 7. But the second series is of matching geometry is built from the variants of diamond elements shown in Figure 8. In this figure, white circles denote primal nodes and the grey circles denote dual nodes. The particular element advocated in the present study is the `2P1P0` diamond element, i.e. the fourth element in Figure 8.

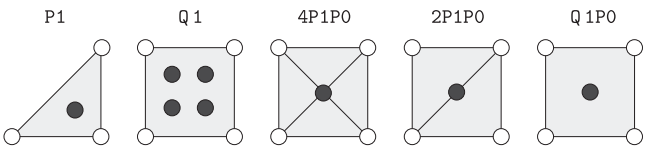

Figure 7. Two-dimensional square elements considered in numerical tests.

DOI: 10.1002/nme

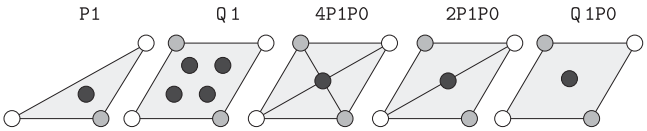

Figure 8. Different variants of two-dimensional diamond elements. The optimal diamond element is `2P1P0`.

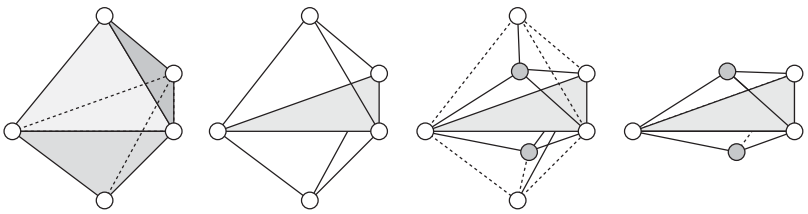

Figure 9. Construction of three-dimensional diamond elements.

The `4P1P0`, `2P1P0` and `Q1P0` elements are expected to exhibit comparable convergence behaviour since they are all based on patchwise averaging. Note, however, that there is a fundamental difference between an *a posteriori* pressure averaging, as typically applied to the standard `4P1P0` or `4CST` crossed-triangle element, and *a priori* averaging as applied to the `2P1P0` and the `Q1P0` element. The latter two are more stable in calculations because high local pressure oscillations are precluded *ab initio*. Indeed, in calculations the *a priori* averaging of the Jacobian of the `2P1P0` and `Q1P0` element and the *a posteriori* averaging of the pressure of the `4P1P0` element yield markedly different results.

Figure 9 illustrates the generation of a three-dimensional diamond from the simplicial mesh defined by the white primal nodes. We begin by introducing the grey dual nodes and performing a subdivision of each tetrahedron into four sub-tetrahedra. Each resulting three-dimensional diamond element (cf. Figure 9, right) consists of three white primal nodes and two grey dual nodes whence the deformation field is interpolated. The generation of diamond elements in two dimensions can be effected likewise: by introducing dual nodes in every primal triangle; subdividing every primal triangle into three sub-triangles; and joining pairs of sub-triangles sharing a common primal edge. The volumetric deformation and pressure are taken to be uniform over every diamond element. The termination of the diamond mesh at the boundary is accomplished by means of individual sub-elements, i.e. sub-triangles in two dimensions and sub-tetrahedra in three dimensions. In consequence, the boundary of the diamond mesh consists entirely of primal faces.

Intuitively, one could conclude that the introduction of the additional dual nodes increases the complexity of the problem. However, the convergence studies presented in the following show that the extra cost of the additional dual nodes is largely compensated for by an improvement of the interpolation and thus by faster convergence.

4.3. Two-dimensional Cook's membrane problem

Our first example concerns the classical benchmark problem of Cook's membrane (cf., e.g. Simo and Rifai [9], or more recently by De Souza Neto *et al.* [45]). The geometry and loading are

DOI: 10.1002/nme

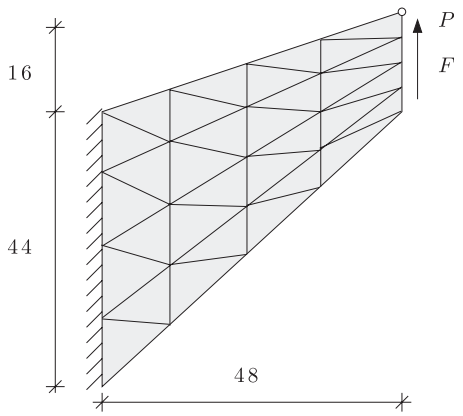

Figure 10. Cook's membrane—geometry and loading conditions.

Table III. Cook's membrane—convergence of top displacement for square meshes.

Elements	dofs	P1	Q1	4P1P0	2P1P0	Q1P0
2×2	18	3.009043	2.113486	2.176959	4.014569	5.509942
4×4	50	3.350305	2.163442	2.747254	5.717503	6.119252
8×8	162	3.592410	2.219074	5.021598	6.492511	6.657711
16×16	578	3.868856	2.380762	6.422618	6.768694	6.829012
32×32	2178	4.381689	2.857057	6.769598	6.867301	6.889818

Table IV. Cook's membrane—convergence of top displacement for diamond meshes.

Elements	dofs	P1	Q1	4P1P0	2P1P0	Q1P0
1.5×1.5	38	3.040019	2.003008	2.419200	4.794911	5.164163
3×3	66	3.459085	2.036571	3.938455	5.457014	6.088334
6×6	202	3.631829	2.136891	6.072108	6.339779	6.667719
12×12	690	3.719908	2.434158	6.711965	6.703881	6.831358
24×24	2530	3.877005	3.105796	6.862243	6.841875	6.890742

shown in Figure 10. The left boundary is fully clamped while the right boundary is subjected to a distributed shearing load $F = 6.25$ per unit length, corresponding to a total vertical resultant force of 100. This load is applied in five increments. Plane strain conditions are assumed. The membrane is assumed to be neo-Hookean, Equation (112), with elastic constants $\mu = 80.1938$ and $\kappa = 400\,942$ resulting in near-incompressible behaviour.

As a basis for comparison, we specifically monitor the vertical displacement of the upper right corner P and its variation upon mesh refinement. The results for regular square meshes and for the special diamond meshes are summarized in Tables III and IV, respectively. The resulting pressure distributions on the deformed configurations are depicted in Figures 11 and 12, with the former corresponding to regular square meshes and the latter to the special diamond meshes.

DOI: 10.1002/nme

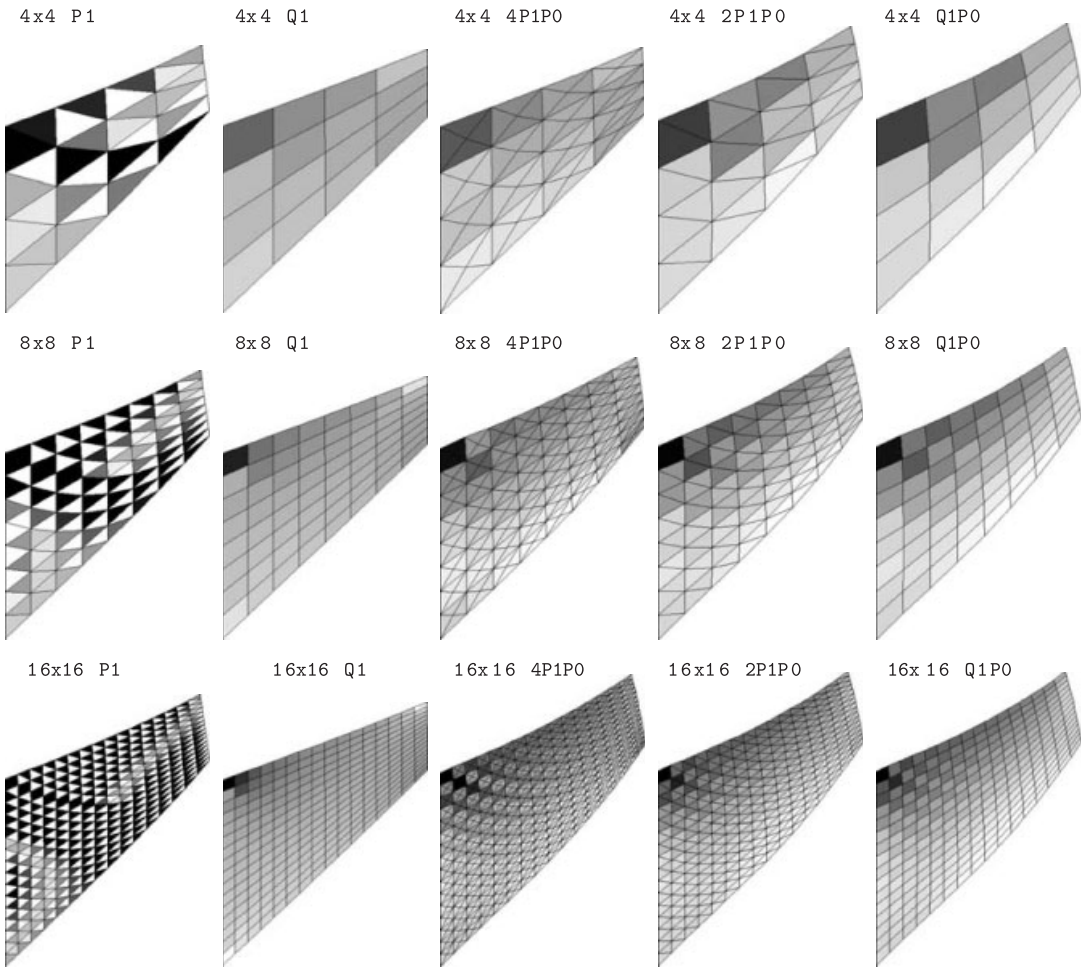

Figure 11. Cook's membrane—hydrostatic pressure for square meshes.

As expected, the response of the standard `P1` and `Q1` element is overly stiff for the constrained problem under consideration. Indeed, the standard elements exhibit typical locking behaviour in both the regular and the diamond configurations. In addition, the `P1` element suffers from severe checkerboarding, which is also visible but less pronounced in the standard `Q1` element. As expected from analysis, the performance of the patchwise averaging elements, i.e. the `4P1P0` element, the `2P1P0` element and the `Q1P0` element, is quite similar. In particular, the vertical displacements of point P are nearly identical in all three cases and converge upon mesh refinement.

This displacement convergence notwithstanding, on the square meshes the `4P1P0`, `2P1P0` and `Q1P0` elements exhibit a marked tendency towards checkerboarding. Moreover, the spurious checkerboard modes do not vanish upon mesh refinement. The resulting strong pressure oscillations between patches are clearly visible in the third, fourth and fifth columns in Figure 11. By way of contrast, the diamond meshes are free of checkerboarding instabilities. Indeed, in the diamond

DOI: 10.1002/nme

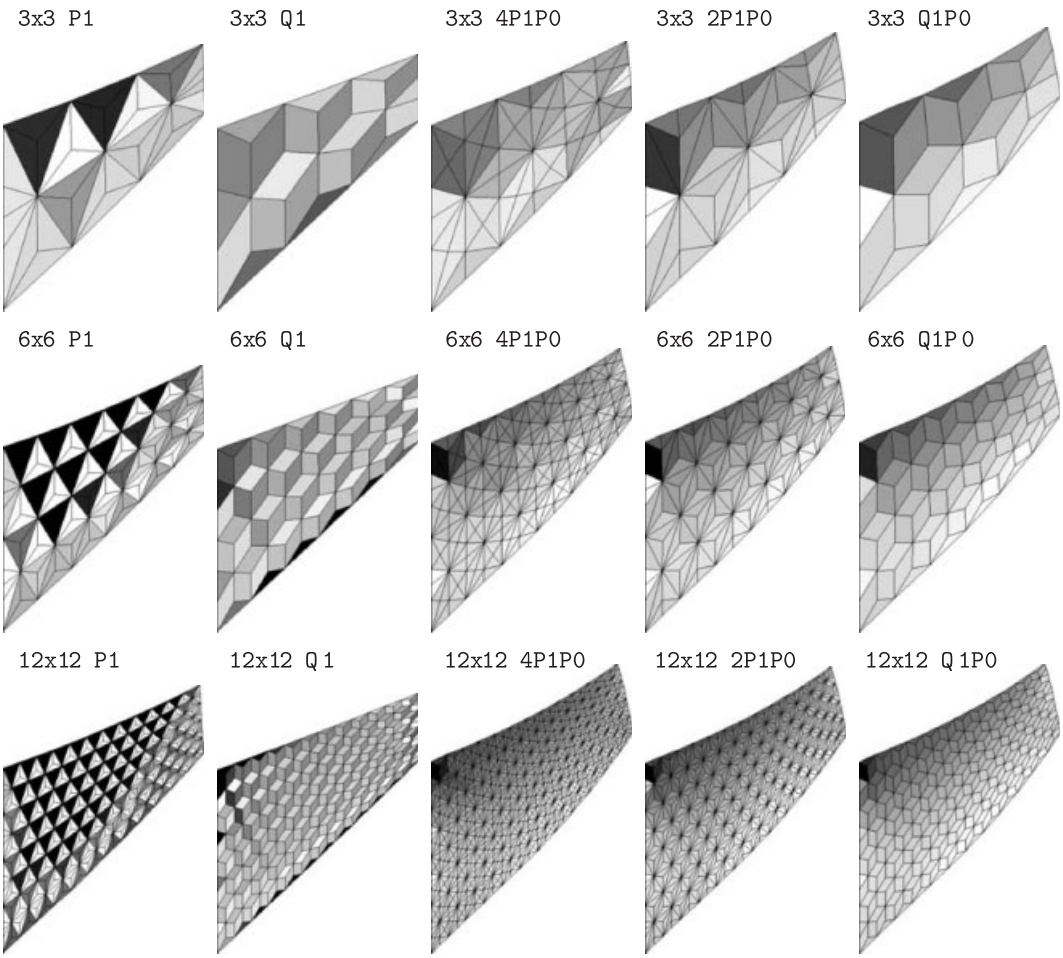

Figure 12. Cook's membrane—hydrostatic pressure for diamond meshes.

configuration the `4P1P0`, `2P1P0` and `Q1P0` elements, depicted in columns three, four and five of Figure 12, result in smooth pressure distributions. These tests thus suggest that diamond elements are indeed free of checkerboard modes even in the finite-deformation range.

4.4. Two-dimensional rigid flat punch

Our second example concerns the benchmark problem of a rigid flat punch (cf. Kikuchi [18], or more recently De Souza Neto *et al*. [45]). The geometry of the problem and the loading conditions are shown in Figure 13. In a plane strain analysis, we study the deformation of a rectangular rubber block in response to frictionless indentation. The block is nearly incompressible elastic with $\mu = 80.1938$ and $\kappa = 400\,942$. The vertical displacement of the indenter is increased incrementally up to a 12.5% compression.

DOI: 10.1002/nme

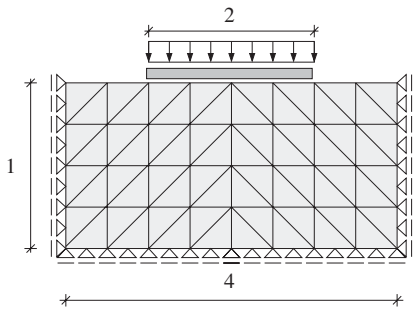

Figure 13. Rigid flat punch—geometry and loading conditions.

Table V. Rigid flat punch—convergence of forces for square meshes.

Elements	dofs	P1	Q1	4P1P0	2P1P0	Q1P0
2 × 8	54	30 238.2325	37 434.9309	415.3908	378.6230	314.8409
4 × 16	170	5506.5734	12 814.9798	351.3208	325.4552	297.4452
6 × 24	350	2928.0829	6384.5861	324.3814	309.0326	291.1465
8 × 32	594	2090.2477	3879.1036	309.2214	300.6662	287.4644
12 × 48	1274	1347.6298	1980.0245	289.3809	291.6279	282.8515
16 × 64	2210	1060.4881	1285.6713	282.1153	286.4848	280.0719

Table VI. Rigid flat punch—convergence of forces for diamond meshes.

Elements	dofs	P1	Q1	4P1P0	2P1P0	Q1P0
2 × 12	120	11 387.8033	44 405.9041	503.0786	319.2090	573.6443
4 × 24	382	6046.6683	6933.9893	307.1889	311.2500	291.9958
6 × 36	788	2366.3477	4615.6062	346.2629	296.9387	334.0307
8 × 48	1338	2034.5728	2195.1990	285.8353	289.8386	279.0617
12 × 72	2870	1219.8163	1222.6799	279.6504	283.0907	275.1793

Tables V and VI summarize the convergence behaviour of the resultant force under mesh refinement for meshes in square and diamond configurations, respectively. As before, in both cases the P1 and the Q1 elements exhibit severe locking behaviour and the predicted response is overly stiff. Consistent with analysis, the 4P1P0, 2P1P0 and Q1P0 elements display nearly identical resultant-force convergence behaviour.

By way of contrast, the pressure fields computed in the square and diamond configurations differ markedly, Figure 14. Thus, whereas the averaged pressure elements, i.e. the 4P1P0, 2P1P0 and Q1P0 elements, exhibit strong checkerboarding in the square–mesh configuration, in the diamond configuration the 4P1P0, 2P1P0 and Q1P0 elements are entirely free from spurious checkerboarding. In particular, the 2P1P0 element may be regarded as an optimal choice in as much as it is simultaneously free of locking and checkerboarding.

DOI: 10.1002/nme

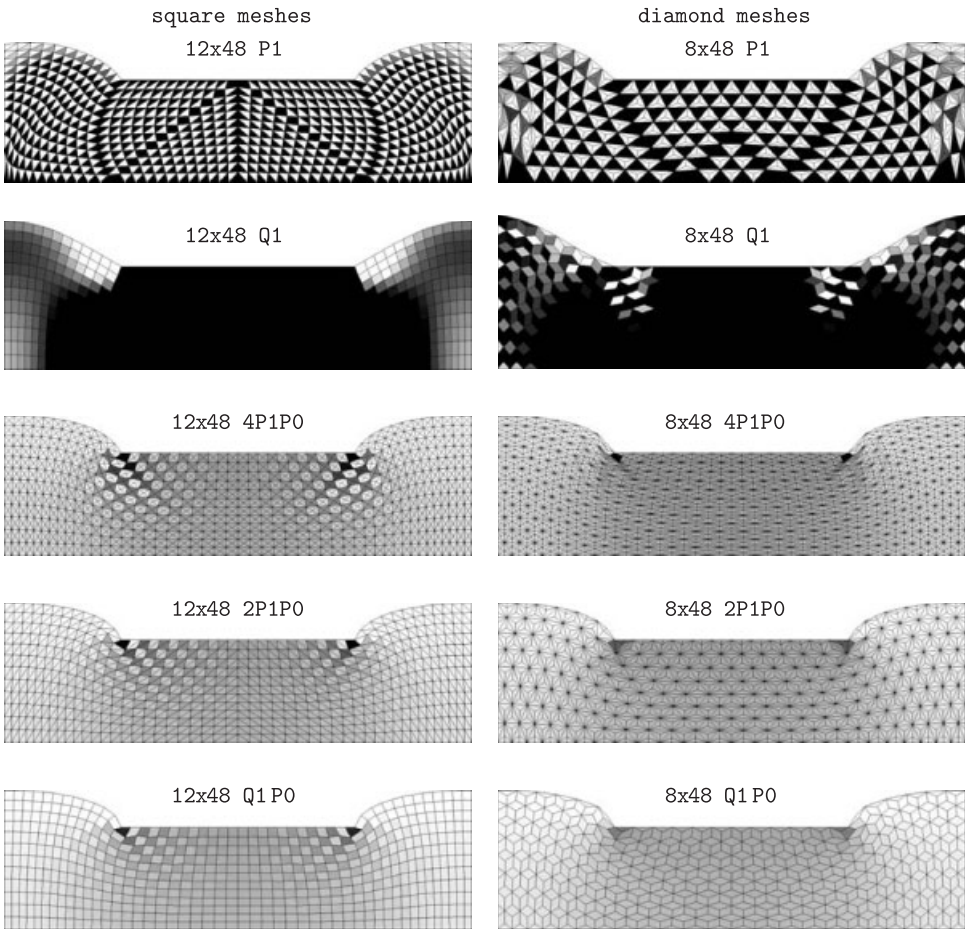

Figure 14. Rigid flat punch—deformed configurations and hydrostatic pressure.

4.5. Three-dimensional compression of a square block

One of the appealing features of diamond elements is that they can be defined in any dimension. We proceed to demonstrate this feature by means of the example of a three-dimensional elastic block indented by a frictionless and rigid square punch (cf., e.g. Reese and Wriggers [47]). We assume near-incompressible elastic behaviour with $\mu = 80.1938$ and $\kappa = 400\,942$. The boundary conditions and the applied forces are shown in Figure 15.

We analyse four different meshes containing 661, 2047, 4649 and 8851 primal nodes and 3072, 10 368, 24 576 and 48 000 dual nodes, respectively. The four meshes considered consist of 5670, 19 872, 47 616 and 93 600 diamond elements inside the domain and 768, 1728, 3072 and 4800 tetrahedra on the boundary. The resulting number of degrees of freedom is 11 199, 37 245, 87 675 and 170 553, respectively.

DOI: 10.1002/nme

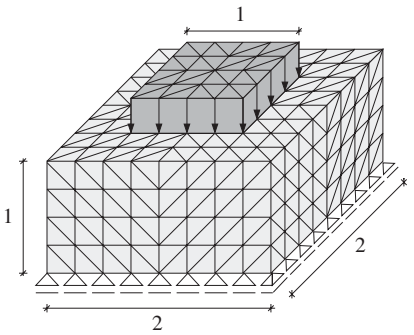

Figure 15. Three-dimensional compression—geometry and loading conditions.

The deformed configurations corresponding to a compression of 12.5% are depicted in Figure 16. The left column of the figure shows the boundary tetrahedra, while the right column shows the corresponding diamond elements. The pressure field is shown in grey scale. Convergence upon mesh refinement is assessed in terms of the resultant force corresponding to a punch travel of 0.125. As expected, the applied force resultant decreases with mesh refinement. Thus, the force resultant is computed to be `45.0470` for the coarsest mesh; `42.8267` for the second mesh; `41.7038` for the third mesh; and `41.1025` for the finest mesh. For all four discretizations, the diamond meshes result in smooth oscillation-free pressure distributions. The three-dimensional analysis is thus consistent with the previous two-dimensional analyses and suggests that the convergence properties of diamond elements are identical in all spatial dimensions. In particular, as in the two-dimensional case the `2P1P0` elements are optimal in the sense of simultaneously being locking-free and free of checkerboard modes.

5. SUMMARY AND CONCLUSION

We have presented a finite element discretization scheme for the compressible and incompressible elasticity problems based on considerations of topology and analysis. The scheme combines a special mesh or 'tiling' pattern into *diamond elements* and a choice of interpolation that guarantee optimal convergence of displacements and pressures. In particular, we have shown that the scheme satisfies the inf–sup condition in the context of linearized kinematics. The attendant checkerboard-free convergence of the pressure field has also been demonstrated in the finite-deformation range by way of numerical testing. Additional desirable features of the diamond discretization scheme include its definition for arbitrary unstructured triangulations of the domain and in general spatial dimension.

We close by pointing out a number of open questions and directions for further study. In the present work, we have exhibited *one* special mesh topology that, in conjunction with appropriate interpolation space, guarantees the satisfaction of the inf–sup condition. A much stronger result, which would bring closure to the subject, would consist of the complete enumeration of *all* such special topologies.

More generally, we remark that there is an extensive literature on algebraic topology which bears in obvious ways on questions of computational mechanics but which has made limited inroads

DOI: 10.1002/nme

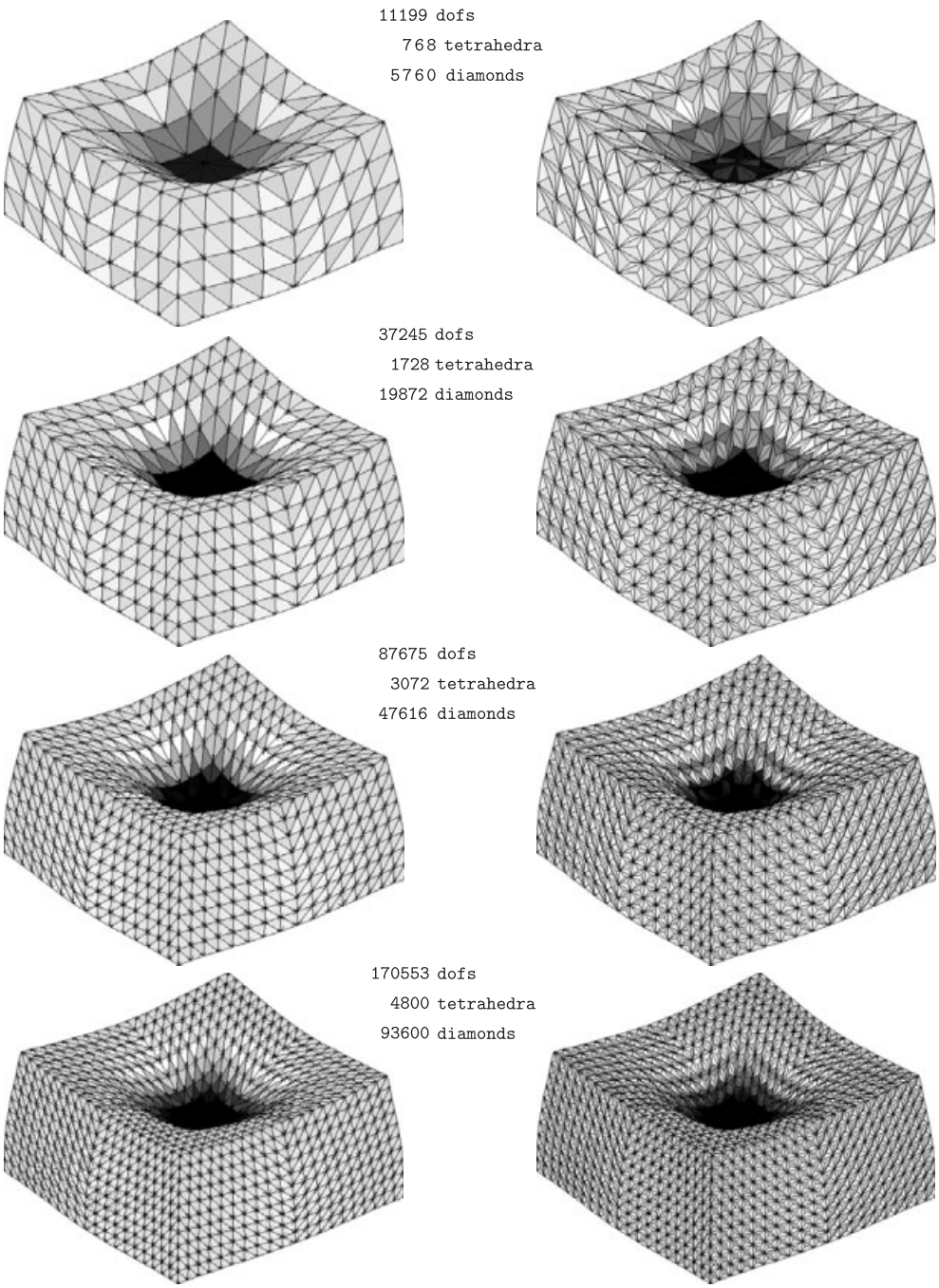

Figure 16. Three-dimensional compression—hydrostatic pressure for diamond meshes.

DOI: 10.1002/nme

into the field. Discrete mechanics is an unfolding current attempt at strengthening the connection between algebraic topology, exterior calculus and mechanics. Discretization schemes inspired in discrete calculus have been successful in *vector* problems such as electromagnetism. By way of contrast, they have been less successful in the context of *tensor* problems such as elasticity. Indeed, locking and checkerboard phenomena do not arise in scalar problems but are quintessential features of vector problems in the presence of internal constraints. Counterexamples (cf., e.g. [34]) show that the mere ability to express an approximation scheme in terms of discrete differential operators does not ensure that the scheme is locking and checkerboard-free and optimally convergent. This cautionary note notwithstanding, there is a close connection between the classical inf–sup condition and the cohomology of the discrete tensor differential complex (cf. Proposition 4), which shows that the topology of the discretization plays an important role in determining convergence. We thus may conclude that both considerations of topology and analysis are essential in the design of discretization schemes and that neither suffices to guarantee the optimal performance of the scheme.

ACKNOWLEDGEMENTS

We gratefully acknowledge the support of the Department of Energy through Caltech's ASCI/ASAP Center for Simulating the Dynamic Response of Materials.

REFERENCES

1. Ladyzhenskaya OA. *The Mathematical Theory of Viscous Incompressible Flows*. Gordon and Breach: New York, 1969.
2. Babuška I. The finite-element method with Lagrangian multipliers. *Numerische Mathematik* 1973; **20**:179–182.
3. Brezzi F. On the existence, uniqueness and approximation of saddle-point problems arising from Lagrangian multipliers. *RAIRO Analyse Numérique*, *Série Rouge* 1974; **8**:129–151.
4. Crouzeix M, Raviart P-A. Conforming and nonconforming finite element methods for solving the stationary Stokes equation. *RAIRO* 1973; **3**:33–75.
5. Bercovier M, Pironneau O. Error estimates for finite element solution of the Stokes problem in the primitive variables. *Numerische Mathematik* 1979; **33**:211–224.
6. Verfürth R. Error estimate for a mixed finite element approximation of the Stokes equation. *RAIRO Analyse Numérique* 1984; **18**(2):175–182.
7. Arnold DN, Brezzi F, Fortin M. A stable finite element for the Stokes equations. *Calcolo* 1984; **21**:337–344.
8. Hughes TJR. Generalization of selective integration procedures to anisotropic and nonlinear media. *International Journal for Numerical Methods in Engineering* 1980; **15**:1413–1418.
9. Simo JC, Rifai MS. A class of mixed assumed strain methods and the method of incompatible modes. *International Journal for Numerical Methods in Engineering* 1990; **29**:1595–1638.
10. Braess D, Carstensen C, Reddy BD. Uniform convergence and a posteriori error estimators for the enhanced strain finite element method. *Numerische Mathematik* 2004; **96**:461–479.
11. Lamichhane B, Reddy D, Wohlmuth B. Convergence in the incompressible limit of finite element approximations based on the Hu-Washizu formulation. *Technical Report 2004-05*, Stuttgart University, 2004.
12. Stenberg R. Error analysis of some finite element methods for the Stokes problem. *Mathematics of Computation* 1990; **54**:495–508.
13. Girault V, Raviart P-A. *Finite Element Methods for Navier–Stokes Equations*: *Theory and Algorithms*. Springer: Berlin, 1986.
14. Ern A, Guermond J-L. *Theory and Practice of Finite Elements*. Applied Mathematical Series, vol. 159. Springer: New York, 2004.
15. Brezzi F, Fortin M. Mixed and hybrid finite element methods. *Springer Series in Computational Mathematics*, vol. 15. Springer: New York, 1991.

DOI: 10.1002/nme

16. Nagtegaal JC, Parks DM, Rice JR. On numerical accurate finite element solutions in the fully plastic range. *Computer Methods in Applied Mechanics and Engineering* 1974; **4**:153–177.
17. Mercier B. A conforming finite element method for two-dimensional incompressible elasticity. *International Journal for Numerical Methods in Engineering* 1979; **14**:942–945.
18. Kikuchi N. Remarks on 4CST-elements for incompressible materials. *Computer Methods in Applied Mechanics and Engineering* 1983; **37**:109–123.
19. Le Tallec P. Compatibility condition and existence results in discrete finite incompressible elasticity. *Computer Methods in Applied Mechanics and Engineering* 1981; **27**:239–259.
20. Boland J, Nicolaides RA. Stability of finite elements under divergence constraint. *SIAM Journal on Numerical Analysis* 1983; **20**(4):722–731.
21. Boland J, Nicolaides RA. Stable and semistable low order finite elements for viscous flows. *SIAM Journal on Numerical Analysis* 1985; **22**:474–492.
22. Stenberg R. Analysis of mixed finite element methods for the Stokes problem: a unified approach. *Mathematics of Computation* 1984; **42**:9–23.
23. Stenberg R. A technique for analysing finite element methods for viscous incompressible flow. *International Journal for Numerical Methods in Fluids* 1990; **11**:935–948.
24. Kröner E. Allgemeine kontinuumstheorie der versetzungen und eigenspannungen. *Archive for Rational Mechanics and Analysis* 1959; **4**:273–334.
25. Bossavit A. *Electromagntisme*, *en vue de la modlisation*. Springer: New York, 1993.
26. Bossavit A. *Computational Electromagnetism. Variational Formulation*, *Complementarity*, *Edge Elements*. Academic Press: San Diego, 1998.
27. Hiptmair R. Finite elements in computational electromagnetism. *Acta Numerica*, vol. 11. Cambridge University Press: Cambridge, 2002; 237–339.
28. Hirani A. Discrete exterior calculus. *Ph.D. Thesis*, California Institute of Technology, 2003.
29. Leok M. Foundations of Computational Geometric Mechanics. *Ph.D. Thesis*, California Institute of Technology, 2003.
30. Arnold DN, Winther R. Mixed finite elements for elasticity. *Numerische Mathematik* 2002: 401–419.
31. Arnold DN. Differential complexes and numerical stability. *Proceedings of the International Congress of Mathematicians*, *volume I*: *Plenary Lectures*, Beijing, 2002.
32. Arnold DN, Falk RS, Winther R. Differential complexes and stability of finite element methods ii: the elasticity complex. *Proceedings of the IMA Workshop on Compatible Spatial Discretizations for PDE*, preprint downloadable at http://ima.umn.edu/~arnold/, 2005, to be submitted.
33. Arnold DN, Falk RS, Winther R. Differential complexes and stability of finite element methods ii: the de Rham complex. *Proceedings of the IMA Workshop on Compatible Spatial Discretizations for PDE*, preprint downloadable at http://ima.umn.edu/~arnold/, 2005, to be submitted.
34. Hauret P, Kuhl E, Ortiz M. Discrete differential operators and analysis in incompressible elasticity, in press.
35. Lions J-L, Magenes E. *Non Homogeneous Boundary Value Problems and Applications*. Springer: New York, 1972.
36. Bernardi C, Maday Y, Patera AT. Domain decomposition by the mortar element method. In *Asymptotic and Numerical Methods for Partial Differential Equations with Critical Parameters*, Kaper HG, Garbey M (eds). Kluwer Academic Publishers: N.A.T.O. ASI, 1993; 269–286.
37. Ben Belgacem F. The mortar finite element method with Lagrange multipliers. *Numerische Mathematik* 1999; **84**:173–197.
38. Wohlmuth BI. *Discretization Methods and Iterative Solvers Based on Domain Decomposition*. Springer: Berlin, 2001.
39. Hauret P. Méthodes numériques pour la dynamique des structures non-linéaires incompressibles à deux échelles (Numerical methods for the dynamic analysis of two-scale incompressible non-linear structures). *Ph.D. Thesis*, Ecole Polytechnique, 2004.
40. Ruas V. A mixed method of the stress–displacement pressure type for solving incompressible plane–strain viscoelasticity problems. *Comptes Rendus à l'Académie des Sciences Paris* 1985; **II**(301):1171–1174.
41. Bott R, Tu LW. *Differential Forms in Algebraic Topology*. Springer: New York, 1982.
42. Munkres JR. *Elements of Algebraic Topology*. Perseus Publishing, 1984.
43. Abraham R, Marsden JE, Ratiu T. *Manifolds*, *Tensor Analysis*, *and Applications*. Springer: New York, 1983.
44. Sokolnikoff IS. *Mathematical Theory of Elasticity*. McGraw-Hill: New York, 1946.

DOI: 10.1002/nme

45. De Souza Neto EA, Pires FM, Owen DRJ. F-bar-based linear triangles and tetrahedra for finite strain analysis of nearly incompressible solides. Part i: formulation and benchmarking. *International Journal for Numerical Methods in Engineering* 2005; **62**:353–383.
46. Moran B, Ortiz M, Shih CF. Formulation of implicit finite-element methods for multiplicative finite deformation plasticity. *International Journal for Numerical Methods in Engineering* 1990; **29**(3):483–514.
47. Reese S, Wriggers P. A stabilization technique to avoid hourglassing in finite elasticity. *International Journal for Numerical Methods in Engineering* 2000; **48**:79–109.

DOI: 10.1002/nme